# Unbalanced emission reductions of different species and sectors in China during COVID-19 lockdown derived by multi-species surface observation assimilation

Lei Kong[1,3], Xiao Tang[*,1,3], Jiang Zhu[2,3], Zifa Wang[1,3,4], Yele Sun[1,3], Pingqing Fu[5], Meng Gao[6], Huangjian Wu[1,3], Miaomiao Lu[7], Qian Wu[1,3], Shuyuan Huang[8], Wenxuan Sui[1], Jie Li[1,3], Xiaole Pan[1,3], Lin Wu[1,3], Hajime Akimoto[9], Gregory R. Carmichael[10]

[1]State Key Laboratory of Atmospheric Boundary Layer Physics and Atmospheric Chemistry (LAPC), Institute of Atmospheric Physics, Chinese Academy of Sciences, Beijing 100029, China
[2]CAS-TWAS Center of Excellence for Climate and Environment Sciences (ICCES), Institute of Atmospheric Physics, Chinese Academy of Sciences, Beijing 100029, China
[3]University of Chinese Academy of Sciences, Beijing 100049, China
[4]Center for Excellence in Regional Atmospheric Environment, Institute of Urban Environment, Chinese Academy of Sciences, Xiamen 361021, China
[5]Institute of Surface-Earth System Science, Tianjin University, Tianjin 300072, China
[6]Department of Geography, State Key Laboratory of Environmental and Biological Analysis, Hong Kong Baptist University, Hong Kong SAR, China
[7]State Environmental Protection Key Laboratory of Urban Ambient Air Particulate Matter Pollution Prevention and Control, College of Environmental Science and Engineering, Nankai University, Tianjin 300350, China
[8]Chengdu University of Information Technology, Chengdu 610225, China
[9]National Institute for Environmental Studies, Onogawa, Tsukuba 305-8506, Japan
[10]Center for Global and Regional Environmental Research, University of Iowa, Iowa City, IA 52242, USA

*Correspondence to*: Xiao Tang (tangxiao@mail.iap.ac.cn)

**Abstract.** The unprecedented lockdown of human activities during the COVID-19 pandemic have significantly influenced the social life in China. However, understanding of the impact of this unique event on the emissions of different species is still insufficient, prohibiting the proper assessment of the environmental impacts of COVID-19 restrictions. Here we developed a multi-air pollutant inversion system to simultaneously estimate the emissions of $NO_x$, $SO_2$, CO, $PM_{2.5}$ and $PM_{10}$ in China during COVID-19 restrictions with high temporal (daily) and horizontal (15km) resolutions. Subsequently, contributions of emission changes versus meteorology variations during COVID-19 lockdown were separated and quantified. The results demonstrated that the inversion system effectively reproduced the actual emission variations of multi-air pollutants in China during different periods of COVID-19 lockdown, which indicate that the lockdown is largely a nationwide road traffic control measure with $NO_x$ emissions decreased substantially by ~40%. However, emissions of other air pollutants were found only decreased by ~10%, because power generation and heavy industrial processes were not halted during lockdown, and residential activities may actually have increased due to the stay-at-home orders. Consequently, although obvious reductions of $PM_{2.5}$ concentrations occurred over North China Plain (NCP) during lockdown period, the emission change only accounted for 8.6% of $PM_{2.5}$ reductions, and even led to substantial increases of $O_3$. The meteorological variation instead dominated the changes in $PM_{2.5}$ concentrations over NCP, which contributed 90% of the $PM_{2.5}$ reductions over most parts of NCP region. Meanwhile,

37  our results suggest that the local stagnant meteorological conditions together with inefficient reductions in PM$_{2.5}$ emissions
38  were the main drivers of the unexpected PM$_{2.5}$ pollution in Beijing during lockdown period. These results highlighted that
39  traffic control as a separate pollution control measure has limited effects on the coordinated control of O$_3$ and PM$_{2.5}$
40  concentrations under current complex air pollution conditions in China. More comprehensive and balanced regulations for
41  multiple precursors from different sectors are required to address O$_3$ and PM$_{2.5}$ pollution in China.

## 1 Introduction

43  A novel coronavirus disease (COVID-19) broke out in Wuhan at the end of 2019 but quickly spread across the whole
44  China within a month. To curb the spread of the virus, strict epidemic control measures were implemented by Chinese
45  governments to prevent large gatherings, including strict travel restriction, shutting down of non-essential industries, extended
46  holidays, closing of schools and entertainment houses (Cheng et al., 2020). These restrictions have had a significant impact on
47  the industrial activities and social life, as exemplified by the drop of China's industrial output by 15-30%
48  (https://data.stats.gov.cn/, last accessed on 22 Oct, 2022) and the dramatic decrease of traffic flow by 60–90% in major cities
49  of China during COVID-19 epidemic (http://jiaotong.baidu.com/, last accessed on 22 Oct, 2022), which provides us a natural
50  experiment to examine the responses of the emissions and air quality on the changes in human activities.
51  It has been well documented that the short-term stringent emission control targeted on power generator or heavy industry
52  enacted by Chinese government during certain societal events, such as the 2008 Olympics Games, 2014 Asia-Pacific Economic
53  Cooperation conference and 2015 China Victory Day Parade, is an effective way to reduce emissions and improve air quality
54  (Okuda et al., 2011; Wang et al., 2014; Tang et al., 2015; Zhang et al., 2016; Wu et al., 2020; Chu et al., 2018). However,
55  different from those stringent emission controls, the COVID-19 restrictions are inclined to affect emissions from sectors more
56  closely to social life whose influence on emissions has still not well been assessed. Previous studies suggest that the COVID-
57  19 restrictions have substantially reduced the China's anthropogenic emissions from almost all sectors (Zheng et al., 2021;
58  Huang et al., 2021; Xing et al., 2020). For example, by using a bottom-up method based on near-real-time activity data, Zheng
59  et al. (2021) reported that the emissions of NO$_x$, SO$_2$, CO and primary PM$_{2.5}$ decreased by 36%, 27%, 28% and 24% during
60  COVID-19 restrictions, mostly due to the reductions in industry and transportation sector. Xing et al. (2020), by using a
61  response model, estimated stronger COVID-19 shutdown effects on emissions over the North China Plain (NCP) with
62  emissions of NO$_x$, SO$_2$ and primary PM$_{2.5}$ dropped by 51%, 28% and 63%, respectively. Others argue that the COVID-19
63  restriction may mainly affect the emissions from transportation, light industry and manufacturing, while it has much smaller
64  effects on the emissions from the power generator and heavy industry because of their non-interruptible processes (Chu et al.,
65  2021; Hammer et al., 2021; Le et al., 2020; Zhao et al., 2020). Moreover, the residential emissions may even increase during
66  the COVID-19 lockdown due to the increased demanding for space heating and cooking with the stay-at-home orders.
67  Therefore, Le et al. (2020) only considered the NO$_x$ reductions during COVID-19 restrictions in their investigation of the
68  severe haze during COVID-19 lockdown, and similarly, Hammer et al. (2021) only considered the emission reductions in the

69 transportation sector. This indicates that there has large uncertainty in the current understanding of the effects of COVID-19
70 restrictions on the emissions of different species.

71       Quantification of the emission changes of different species and different sectors during the COVID-19 lockdown is thus
72 necessary for the comprehensive understanding of the environmental impacts of COVID-19 restrictions. In particular, although
73 observations indeed show decreases of air pollutant concentrations during COVID-19 restrictions (Fan et al., 2020; Wang et
74 al., 2021; He et al., 2020; Shi and Brasseur, 2020), the air quality improvement is much smaller than the expected (Shi et al.,
75 2021; Diamond and Wood, 2020; Yan et al., 2022). Moreover, severe haze still occurred in northern China (Sulaymon et al.,
76 2021; Le et al., 2020) and $O_3$ concentrations even showed significant increases (Zhang et al., 2021; Li et al., 2020). A number
77 of studies were conducted to explain this anomalistic air quality change by analyzing the effects of emission changes,
78 meteorological variations and secondary production (Huang et al., 2021; Le et al., 2020; Hammer et al., 2021; Zhao et al.,
79 2020; Zhao et al., 2021; Sulaymon et al., 2021; Wang et al., 2020; Li et al., 2021). However, due to the unknown emission
80 changes during COVID-19 restrictions, the emission reduction scenarios that used to represent the COVID-19 shutdown effects
81 varied among different studies and did not consider the spatial and temporal heterogeneity of the emission changes, leading to
82 biases in the model simulation (Zhao et al., 2021; Li et al., 2021; Hammer et al., 2021; Zheng et al., 2021) and uncertainty in
83 the quantification of the contributions of different factors.

84       Pioneer studies by Zheng et al. (2021) and Forster et al. (2020) have derived multi-air pollutant emissions from social
85 activity data using a bottom-up method, but due to the lack of detailed social activity data, large uncertainties existed in their
86 estimates. The meteorologically and seasonally driven variability of the concentrations of air pollutants also prohibit drawing
87 fully quantitative conclusions on the changes of emissions based on observations alone (Levelt et al., 2022). The emission
88 inversion technique, which takes advantage of the chemical transport model (CTM) and real-time observations, provides an
89 attractive way to estimate the sector-specific and space-based emission changes during COVID-19 restrictions, as shown in
90 Zhang et al. (2020), Zhang et al. (2021), Feng et al. (2020) and Hu et al. (2022). However, these studies only inversed the
91 emissions of single species (e.g., $NO_x$ and $SO_2$) without insights into multiple species. In view of this discrepancy, in this study
92 we developed a multi-air pollutant inversion system to simultaneously estimated the multi-air pollutant emissions in China,
93 including $NO_x$, $SO_2$, CO, $PM_{2.5}$ and $PM_{10}$, during the COVID-19 restrictions using an ensemble Kalman filter (EnKF) and
94 surface observations from the China National Environmental Monitoring Centre (CNEMC). Subsequently, the inversed
95 emission inventory was used to quantify the contributions of emission changes versus meteorology variations to the changes
96 in $PM_{2.5}$ and $O_3$ concentrations over the NCP region during the COVID-19 restrictions.

97 **2 Method and data**

98       We developed a high-resolution multi-air pollutant inversion system to estimate the daily emissions of $NO_x$, $SO_2$, CO,
99 $PM_{2.5}$ and $PM_{10}$ in China from 1 Jan to 29 Feb 2020 when the COVID-19 pandemic was at its most serious and the effects of
100 the COVID-19 restrictions were most profound in China. This system uses the NAQPMS (Nested Air Quality Prediction

101 Modelling System) model as the forecast model and the EnKF coupled with the state argumentation method as the inversion
102 method. It has the capabilities of simultaneous inversion of multi-air pollutant emissions at high temporal (daily) and spatial
103 (15km) resolutions. An iteration inversion scheme was also developed in this study to address the large biases in the a priori
104 emissions. In order to better characterize the emission changes during the COVID-19 restrictions, the whole time period was
105 divided into three periods according to different control phases of COVID-19 and the timing of the Chinese Lunar New Year:
106 before lockdown (P1, January 1-20), lockdown (P2, January 21-February 9) and after back-to-work day (P3, February 10-29).
107 Emission changes in different regions of China were also analyzed, including the North China Plain (NCP), Northeast China
108 (NE), Southeast China (SE), Southwest China (SW), Northwest China (NW) and Central regions (defined in Fig. 1) to
109 investigate the responses of emissions to the COVID-19 restrictions in different regions. In the following sections, we briefly
110 introduce each component of the inversion system.

111 **2.1 Chemical transport model and its configuration**

112 The NAQPMS model was used as the forecast model to represent the atmospheric chemistry in this study, which has been
113 used in previous inversion studies (Tang et al., 2011; Tang et al., 2013; Kong et al., 2019; Wu et al., 2020), where detailed
114 descriptions of NAQPMS are available. The Weather Research and Forecasting Model (WRF)(Skamarock, 2008) is used to
115 provide the meteorological inputs to the NAQPMS model.

116 Figure 1 shows the modelling domain of this study with a high horizontal resolution of 15 km. The a priori emission
117 inventory used in this study includes monthly anthropogenic emissions from the HTAP_v2.2 emission inventory for the base
118 year of 2010 (Janssens-Maenhout et al., 2015), biomass burning emissions from the Global Fire Emissions Data base (GFED)
119 version 4 (Randerson et al., 2017; Van Der Werf et al., 2010), biogenic volatile organic compound (BVOC) emissions from
120 MEGAN-MACC (Sindelarova et al., 2014), marine volatile organic compound emissions from the POET database (Granier et
121 al., 2005), soil $NO_x$ emissions from the Regional Emission inventory in Asia (Yan et al., 2003) and lightning $NO_x$ emissions
122 from Price et al. (1997). Chemical top and boundary conditions were provided by the global CTM MOZART (Model for
123 Ozone and Related Chemical Tracers) (Brasseur et al., 1998; Hauglustaine et al., 1998). We assumed no monthly variations in
124 the a priori emission inventory and used January's emission inventory for the whole simulation period so that the emission
125 variation was solely derived from the surface observations. A two-week free run of NAQPMS was conducted as a spin-up
126 time. For each day's meteorological simulation, a 36-h free run of WRF was conducted, of which the first 12-h simulation was
127 a spin-up run and the next 24-h simulation provided the meteorological inputs to NAQPMS. Initial and boundary conditions
128 for the meteorological simulation were provided by the National Center for Atmospheric Research/National Center for
129 Environment Prediction (NCAR/NCEP) 1° ×1° reanalysis data. Evaluation results for the WRF simulation are available in
130 Text S1 in Supplement.

## 2.2 Surface Observations

The hourly concentrations of $NO_2$, $SO_2$, CO, $PM_{2.5}$ and $PM_{10}$ from CNEMC were used in this study to estimate the emissions during COVID-19. The spatial distributions of these observation sites are shown in Fig. 1, which contains 1436 observation sites covering most regions of China. Before assimilation, outliers of observations were first filtered out using the automatic outlier detection method developed by Wu et al. (2018) to prevent the adverse effects of the outliers on data assimilation. Then, the hourly concentrations were averaged to the daily values for the inversions of daily emissions.

The observation error is one of the key inputs to the data assimilation, which together with the background error determine the relative weights of the observation and background values on the analysis. The observation error includes measurement error and representativeness error. The measurement error of each species was designated according to the officially released documents of the Chinese Ministry of Ecology and Environmental Protection (HJ 193-2013 and HJ 654-2013, available at http://www.cnemc.cn/jcgf/dqhj/, last accessed on 22 Oct 2022), which is 5% for $PM_{2.5}$ and $PM_{10}$ and 2% for $SO_2$, $NO_2$ and CO. A representativeness error arises from the different spatial scales that the discrete observation data and model simulation represent, which was estimated based on the previous study by Li et al. (2019) and Kong et al. (2021). It should be noted that the $NO_2$ measurement from CNEMC is made by the chemiluminescent analyser with a molybdenum converter. Due to the interference of $HNO_3$, PAN and alkyl nitrates (AN), the $NO_2$ concentrations can be overestimated (Dunlea et al., 2007; Lamsal et al., 2008) that may lead to spurious decreases in $NO_x$ emissions during the lockdown period. Previous studies usually use chemical transport model to simulate $NO_x$, $HNO_3$, PAN and AN to produce correction factors (CFs) for the $NO_2$ measurements (Cooper et al., 2020; He et al., 2022) using the following relationship proposed by Lamsal et al. (2008):

$$CF = \frac{[NO_2]}{[NO_2]+0.95[PAN]+0.35[HNO_3]+\sum[AN]} \tag{1}$$

but the calculation of CF could be affected by the simulation errors in the model caused by uncertainties in emission inventory or other error sources, which may contaminate the observations. Therefore, similar to Feng et al. (2020), we did not correct the $NO_2$ measurement in our inversion of $NO_x$ emissions since there were large uncertainties in the $NO_x$ emissions during the COVID-19 pandemic that possibly led to erroneous CF. Since the EnKF considered the errors in observations through the use of observation error covariance matrix, the chemiluminescence monitor interference to $NO_2$ measurement were treated as the observation error during the assimilation. A sensitivity inversion experiment was also conducted based on the corrected $NO_2$ measurement using CF, which suggests that the chemiluminescence monitor interference only have small impacts on the inversed $NO_x$ emission in terms of magnitude and its variation during COVID-19 pandemic. Detailed results of the sensitivity experiment are available in Text S2 in Supplement.

## 2.3 Inversion estimation scheme

The EnKF coupled with the state augmentation method was used in this study to constrain the emissions of multiple species. EnKF is an advanced data assimilation method proposed by Evensen (1994) that features representation of the uncertainties of the model state by a stochastic ensemble of model realizations. Different from the mass balance method used

163 in Zhang et al. (2020) and Zhang et al. (2021) that has difficulties in accounting for nonlinear relationship between emissions

164 and concentrations and is more suitable for short-lived species (e.g. $NO_x$) under relatively coarse (>1°) resolutions (Streets et

165 al., 2013), the EnKF can consider the indirect relationship between emissions and concentrations caused by complex physical

166 and chemical processes in the atmosphere through the use of flow-dependent background error covariance produced by

167 ensemble CTM forecasts (Evensen, 2009; Miyazaki et al., 2012). Compared with the four-dimensional variational assimilation

168 method used in Hu et al. (2022), the EnKF method has comparable computational cost (Skachko et al., 2014) but is more easily

169 implemented without the need to develop complicated adjoint models for complex CTMs. The state augmentation method is

170 a commonly used parameter estimation method (Tandeo et al., 2020), in which the emissions of multi species are treated as

171 state variable and are simultaneously updated according to the relationship between the emissions and concentrations of related

172 species. Due to the chemical reactions in the atmosphere, the concentrations of different species are interrelated with each

173 other. For example, the ambient $PM_{2.5}$ is not only primarily emitted, but also formed secondarily through reactions with several

174 gaseous precursors, such as $NO_2$ and $SO_2$. This means that the estimations of $PM_{2.5}$ emission by single inversed estimation

175 method could be biased if the errors in $NO_2$ and $SO_2$ emissions were not corrected synchronously. Therefore, it is beneficial

176 to do the multi-species inversion estimation which can provide more constraints on the atmospheric chemical system and lead

177 to more reasonable inversion results. Meanwhile, the use of EnKF method coupled with the state augmentation method allows

178 the estimations of multi-species emissions almost without additional computational cost.

179      Appropriate estimation of the uncertainty in emissions and chemical concentrations is important for the performance of

180 inversion estimation using EnKF. Since the source emission data over mainland China in HTAP_v2.2 inventory is obtained

181 from the MIX inventory (Li et al., 2017b) , the uncertainties of emissions of different species, including PMF, PMC, BC, OC,

182 $NO_x$, CO, $SO_2$, $NH_3$ and NMVOC (nonmethane volatile organic compounds), were obtained from Li et al. (2017b) and Streets

183 et al. (2003), which were represented by an ensemble of perturbed emissions generated by multiplying the a priori emissions

184 with a perturbation factor $\beta_{i,s}$:

185 $$E_{i,s} = \beta_{i,s} \circ E_s^p, \ i = 1,2, \cdots N_{ens}$$ (2)

186 where $E_{i,s}$ represents the vector of the $ith$ member of perturbed emissions for species $s$, $E_s^p$ represents the a priori emissions

187 for this species, $\circ$ denotes the schur product and $N_{ens}$ denotes the ensemble size. In this way, the adjustment of emissions is

188 equivalent to the adjustment of perturbation factors.

189      In terms of the uncertainty in chemical concentrations, considering that emission uncertainty is the major contributor to

190 the uncertainties in air quality modelling, especially during the COVID-19 period when emissions changed rapidly,

191 uncertainties in chemical variables were obtained through ensemble simulations driven by perturbed emissions. The ensemble

192 size was chosen as 50 to maintain the balance between the filter performance and computational cost. After the ensemble

193 simulations, emissions of multiple species were updated using a deterministic form of EnKF (DEnKF) proposed by Sakov and

194 Oke (2008), which is formulated by

195 $$\overline{x^a} = \overline{x^b} + P_e^b H^T \left( H P_e^b H^T + R \right)^{-1} \left( y^o - H \overline{x^b} \right)$$ (3)

196 $\overline{x^b} = \frac{1}{N}\sum_{i=1}^{N} x_i^b \, ; X_i^b = x_i^b - \overline{x^b}$ (4)

197 $\mathbf{P_e^b} = \frac{1}{N-1}\sum_{i=1}^{N} X_i^b (X_i^b)^{\mathrm{T}}$ (5)

198  where $x$ denotes the state variables; $b$ the background state (a priori); $a$ the analysis state (posteriori); $\mathbf{P_e^b}$ the ensemble-

199  estimated background error covariance matrix and $N$ the ensemble size. $y^o$ represents the vector of observations with an error

200  covariance matrix of $\mathbf{R}$. $\mathbf{H}$ is the linear observational operator that maps the m-dimensional state vector $x$ to a p- (number of

201  observations) dimensional observational vector ($\mathbf{H}\overline{x^b}$). The state variables were defined as follows according to state

202  augmentation method during the assimilation:

203 $x_i = [c_i, \ \beta_i]^T, i = 1,2, \cdots N_{ens}$ (6)

204 $c_i = [PM_{2.5}, PM_{10-2.5}, \ NO_2, \ SO_2, CO]_i$ (7)

205 $\beta_i = [\beta_{PMF}, \beta_{BC}, \ \beta_{OC}, \ \beta_{PMC}, \beta_{NO_x}, \beta_{SO_2}, \beta_{CO}]_i$ (8)

206  where $x_i$ represents the $ith$ member of the assimilated state variable, which consists of the fields of chemical variables $c_i$ and

207  emission perturbation factors $\beta_i$. Detailed descriptions of the model state variables are summarized in Table 1. The use of

208  PM$_{10-2.5}$ (PM$_{10}$ minus PM$_{2.5}$) values was aimed to avoid the potential cross-correlations between PM$_{2.5}$ and PM$_{10}$ (Peng et al.,

209  2018; Ma et al., 2019). Moreover, to prevent spurious correlations between non- or weakly related variables, similar to Ma et

210  al. (2019) and Miyazaki et al. (2012), state variable localization was used during assimilation, with observations of one

211  particular species only used in the updates of the same species' emission rate. Corresponding relationship between the chemical

212  observations and adjusted emissions is summarized in Table 1. The PM$_{2.5}$ observations were one exception and were used to

213  update the emissions of PMF (fine mode unspeciated aerosol), BC (black carbon) and OC (organic carbon) since the

214  observations of speciated PM$_{2.5}$ were not available in this study. The lack of speciated PM$_{2.5}$ observations may lead to

215  uncertainties in the estimated emissions of PMF, BC and OC. Therefore, we only analyzed the emissions of PM$_{2.5,}$ which were

216  the sum of the emissions of these three species. Similarly, only PM$_{10}$ emissions were analyzed in this study, which includes

217  the emissions of PM$_{2.5}$ and PMC (coarse mode unspeciated aerosol).

218     Due to the strict control measures implemented during the last decades, the emissions in China decreased dramatically

219  from 2010 to 2020, especially for SO$_2$. Thus, there are large biases in the a priori estimates of emissions in China (Zheng et

220  al., 2018), which would lead to incomplete adjustments of the a priori emissions and degrade the performance of assimilation.

221  Therefore, an iteration inversion scheme was developed in this study to address the large biases of SO$_2$ emissions. As illustrated

222  in Fig. 2, the main idea of the iteration inversion scheme is to update the ensemble mean of the state variable using the inversion

223  results of the $kth$ iteration and corresponding simulations. The state variable used in the $(k + 1)th$ inversions is written as

224  follows:

225 $x_i^{k+1} = [c^k + c_i^e - \overline{c^e}, \beta^k + \beta_i^e - \overline{\beta^e}]^T$ (9)

226  where $c^k$ represents the simulation results using the inversed emissions of the $kth$ iteration, $c_i^e$ represents the $ith$ member of

227  ensemble simulations with an ensemble mean of $\bar{c}^e$, $\beta^k$ represents the perturbation factors of the $kth$ iteration, and

228  $\beta_i^e$ represents the $ith$ member of the ensemble of perturbation factors with a mean value of $\overline{\beta^e}$.

229      Using this method, the problems of large biases in the a priori emissions were well addressed as exemplified in Fig. 3 for

230  $SO_2$ emissions. It can be clearly seen that due to the large positive biases in the a priori $SO_2$ emissions, the model still has large

231  positive biases (NMB = 30.9–220.5%) and errors (RMSE = 8.7–23.0 μg/m$^3$) in simulated $SO_2$ concentration over all regions

232  of China even after assimilation (first iteration). However, the biases and errors continued to decrease with the increasing of

233  iteration times till the fourth iteration in which there were no significant improvement in $SO_2$ simulations compared to those

234  in third iteration. These results suggested that the iteration inversion method used in this study can well constrain the a priori

235  emission with large biases and, in this application, conducting three iteration is enough for constraining the emission. Besides

236  $SO_2$ emissions, the iteration inversion scheme was also applied to the emissions of other species. Meanwhile, to reduce the

237  influences of random model errors (e.g., errors in meteorological inputs) on the estimation of the variation in emissions, a 15-

238  day running average was performed on our daily inversion results after the inversion estimation.

239  **2.4 Quantification of the effects of emission changes and meteorological variations**

240      In previous studies, the meteorological-induced (MI) changes were usually determined by the CTM with a fixed emission

241  input setting and a varying meteorological input. Then, the difference between the MI changes and total changes in air pollutant

242  concentrations is defined as emission-induced (EI) changes. Another approach to estimate EI changes is to perform simulations

243  with a fixed meteorological input setting and varying emission inputs. Then, the MI changes are defined as the difference

244  between EI changes and total changes in air pollutant concentrations. Due to the nonlinear effects of atmospheric chemical

245  systems, these two methods yield different results. Thus, both methods were used in this study to account for the nonlinear

246  effects. The averaged results of these two methods are used to represent the impacts of emission changes and meteorological

247  variation on the air quality changes during the COVID-19 restrictions. In total, three scenario experiments were designed based

248  on our inversion results (Table 2). The first scenario simulation used the varying meteorological and emission inputs from the

249  P1 to P2 period, which represents the real-world scenario and is used to estimate the total changes in air pollutant concentrations

250  induced by emissions and meteorological changes from the P1 to P2 period (BASE scenario). The second scenario experiment

251  used the varying meteorological inputs but replaced the emissions during the P2 period with those during the P1 period, which

252  was used to estimate the MI changes using the first method (MET change scenario). The third scenario experiment used the

253  varying emissions input and replaced the meteorological input during the P2 period with that during the P1 period, which was

254  used to estimate the EI changes using the second method (EMIS change scenario). Based on the first method, the MI and EI

255  changes can be estimated as follows:

256  $MI_{MET\ change\ scenario} = conc_{p2,MET\ change\ scenario} - conc_{p1,MET\ change\ scenario}$                    (10)

257  $EI_{MET\ change\ scenario} = conc_{p2,BASE\ scenario} - conc_{p1,BASE\ scenario} - MI_{MET\ change\ scenario}$                    (11)

where $MI_{MET\ change\ scenario}$ represents the MI changes estimated based on the results from the MET change scenario, $conc_{p1,MET\ change\ scenario}$ and $conc_{p2,MET\ change\ scenario}$ represent the averaged concentrations of air pollutants during the P1 and P2 periods under the MET change scenario, $EI_{MET\ change\ scenario}$ represents the EI changes estimated based on the results from the MET change scenario, and $conc_{p1,BASE\ scenario}$, $conc_{p2,BASE\ scenario}$ respectively represent the averaged concentrations of air pollutants during the P1 and P2 periods under the BASE scenario. Similarly, the MI and EI changes estimated based on the second method are formulated as follows:

$$EI_{EMIS\ change\ scenario} = conc_{p2,EMIS\ change\ scenario} - conc_{p1,EMIS\ change\ scenario} \tag{12}$$

$$MI_{EMIS\ change\ scenario} = conc_{p2,BASE\ scenario} - conc_{p1,BASE\ scenario} - EI_{EMIS\ change\ scenario} \tag{13}$$

Then, the estimations from these two methods are averaged to estimate the contributions of meteorological change and emission change to the changes in PM$_{2.5}$ and O$_3$ concentrations during the COVID-19 lockdown:

$$MI = (MI_{EMIS\ change\ scenario} + MI_{MET\ change\ scenario})/2 \tag{14}$$

$$EI = (EI_{EMIS\ change\ scenario} + EI_{MET\ change\ scenario})/2 \tag{15}$$

$$contri_{met} = \frac{MI}{MI+EI} \times 100 \tag{16}$$

$$contri_{emis} = \frac{EI}{MI+EI} \times 100 \tag{17}$$

where $contri_{met}$ and $contri_{emis}$ represent the relative contributions (%) of the meteorological variations and emission changes to the changes in air pollutant concentrations. Detailed definition of each notation used in the calculation of MI and EI is given in Table 3.

## 3 Results

### 3.1 Validation of the inversion results

We firstly validate our inversion system by using a cross-validation method, in which 20% of observation sites were withheld from the emission inversion and used as the validation datasets. Figure S1–6 showed the concentrations of different air pollutants in China from 1$^{st}$ Jan to 29$^{th}$ Feb 2020 obtained from observations at validation sites and simulations using a priori and a posteriori emission. Commonly used statistical evaluation indices, including correlation coefficient (R), mean bias error (MBE), normalized mean bias (NMB) and root of mean square error (RMSE) are summarized in Table S1. The validation results suggest that the posteriori simulation agreed well with the observed concentrations for all species. The large biases in the a priori simulation of PM$_{2.5}$, PM$_{10}$, SO$_2$ and CO were almost completely removed in the a posteriori simulation with NMB about -3.9–15.7% for PM$_{2.5}$, -3.1–11.6% for PM$_{10}$, -12.6–5.3% for NO$_2$, -9.5–6.2% for SO$_2$ and -10–7.6% for CO (Table S1). RMSE values were also significantly reduced in the a posteriori simulation which were 9.1–32.2μg/m$^3$ for PM$_{2.5}$, 12.6–42.4μg/m$^3$ for PM$_{10}$, 5.1–12.3μg/m$^3$ for NO$_2$, 1.2–5.6μg/m$^3$ for SO$_2$ and 0.10–0.46mg/m$^3$ for CO. Moreover, the inversion emission considerably improved the fit to the observed time evolution of air pollutants' concentrations. The R values were

improved for all species in the a posteriori simulation that were up to 0.74–0.94 for $PM_{2.5}$, 0.63 – 0.92 for $PM_{10}$, 0.76–0.94 for $NO_2$, 0.23–0.79 for $SO_2$ and 0.63–0.92 for CO. These results suggest that our inversion results have excellent performance in representing the magnitude and variation of these species' emission in China during COVID-19 restrictions. Model performance in simulating $O_3$ concentration is relatively poor compared to other species although improvement was remarkable in NCP, NE and SE regions. This would be due to the use of outdated emission inventory for base year 2010 and that the emission of non-mental volatile organic compounds (NMVOC), another important precursor for $O_3$, were not constrained in this study. As shown in fig. S7, the NMVOC emissions for base year 2010 were generally lower than those for 2018 except over the SW regions. Considering the increasing trend of NMVOC emissions in China (Li et al., 2019), the underestimates of NMVOC emissions for base year 2020 could be larger. This is in line with the negative biases in the simulated $O_3$ concentrations over these regions.

**3.2 Emission changes of multi-species during COVID-19 restrictions**

**3.2.1 Unbalanced emission changes between $NO_x$ and other species**

The control of COVID-19 began on 23rd January when the Chinese government declared the first level of national responses to public health emergencies, one day before the 2020 Chinese New Year Eve. Figure 4 shows the time evolution of the normalized emission anomaly for different species in China from 1st January to 29th February. The temporal variation in the emission varied largely between $NOx$ and other species. Due to the combined effects of the Spring Festival and COVID-19 lockdown, $NO_x$ emissions decreased continuously at the beginning of January until approximately one week after the implementation of the COVID-19 lockdown, with estimated decreases in $NO_x$ emissions of up to 42.5% from the P1 to P2 period (Table 4). Subsequently, the $NO_x$ emissions stabilized with small fluctuations until the official back-to-work day when the $NOx$ emissions began to increase due to easing of the control measures and the resumption of business. According to inversion estimation, $NO_x$ emissions recovered by 3.9% during the P3 period. These results indicate that the temporal variation in our estimated $NO_x$ emissions agreed well with the timing of the Spring Festival and different control stages of COVID-19. However, for other species (i.e., $PM_{2.5}$, $PM_{10}$, $SO_2$ and CO), although their emissions generally decreased from 1st January to the end of the 2020 Spring Festival holiday, they showed much smaller reductions than the $NO_x$ emissions. The emission reduction for these species was only approximately 7.9-12.1% (Table 4). This is consistent with the inversion results by Hu et al. (2022) who found that $SO_2$ emissions in China decreased only by 9.2% during COVID-19 lockdown. In addition, the emissions of these species quickly rebounded to their normal level just one week after the end of the Spring Festival holiday. As estimated by our inversion results, the $SO_2$ emissions recovered by 7.2% during the P3 period, which was only 2.5% lower than that during the P1 period. The $PM_{2.5}$ and $PM_{10}$ emissions during the P3 period were 3.3% and 43.6% higher, respectively, than those during the P1 period.

Similar results were found in different regions of China (Fig. 5 and Table 5), where the $NO_x$ emissions decreased much more than other species. In addition, unlike the uniform decreases in $NO_x$ emissions in different regions of China (~40%),

there was apparent spatial heterogeneity in the emission changes in $PM_{2.5}$, $PM_{10}$, $SO_2$ and CO (Table 5 and Fig. 6). For example, from the P1 to P2 period, the $PM_{2.5}$ emissions decreased by over 20% in the Central region but only by 8.8% in the NE region. The $PM_{2.5}$ emissions even increased by 5.5% in the NCP region. This may be due to the increased emissions from industry and fireworks according to the field measurements conducted by previous studies (Li et al., 2022; Ma et al., 2022; Zuo et al., 2022; Dai et al., 2020). Based on the measurement of stable Cu and Si isotopic signature and distinctive metal ratios in Beijing and Hebei, Zuo et al. (2022) analyzed the variations in the $PM_{2.5}$ sources during the COVID-19 pandemic, who reported that the primary $PM_{2.5}$ emissions did not decrease in Beijing and Hebei, and that the PM-associated industrial emissions may actually increase during the lockdown period. The increased industrial heat sources detected by Li et al. (2022) based on VIIRS active fire data also supported the increased industrial emissions over the NCP region during lockdown period. Meanwhile, consistent with the field measurements in Beijing and Tianjin conducted by Ma et al. (2022) and Dai et al. (2020), substantial high levels of potassium ($K^+$) and magnesium ($Mg^{2+}$) ion were found over the NCP region during the Spring Festival according to the aerosol chemical composition measurements obtained from CNEMC (Fig. S8). Since $K^+$ and $Mg^{2+}$ are two important fingerprints of the firework emissions, the high levels of $K^+$ and $Mg^{2+}$ suggest that the emissions from fireworks during Spring Festival were also a potential contributor to the increased of $PM_{2.5}$ emissions over the NCP region. In contrast, the SW and central regions exhibited relatively larger emission reductions for these species (Fig. 5 and Table 5) by 12.6–25.9% and 10.6–23.7%, respectively. The emission rebound during the P3 period was more prominent in the SE, central and SW regions (Fig. 5 and Fig. 7), where emissions recovered by 6.0–16.4% for $NO_x$, 7.5–19.8% for $SO_2$, 7.4–13.1% for CO, 12.3–47.7% for $PM_{2.5}$ and 28.6–135.9% for $PM_{10}$ (Table 5). This result is consistent with the earlier degradation of the response level to the COVID-19 virus (from the first level to the second or third level) over these regions (Table S2). In contrast, there were decreases in emissions in the NCP, NE and NW regions. $PM_{2.5}$ emissions were reduced by 9.9% in the NCP region and by 19.2% in the NE region from the P2 to P3 period (Table 5). Moreover, we found that the $PM_{10}$ emissions surged in the NW and central regions, where the $PM_{10}$ emissions during the P3 period were almost two times larger than those during the P2 period (Table 5). However, this finding may be related to the enhanced dust emissions over these two regions rather than the effects of returning to work according to the decreased $PM_{2.5}/PM_{10}$ ratios during the P3 period. According to Fig.S9, the $PM_{2.5}/PM_{10}$ ratio was relatively stable during the P1 and P2 period, but it decreased substantially during the P3 period, from 0.81 to 0.48 over the NW region and from 0.77 to 0.53 over the Central region. A lower $PM_{2.5}/PM_{10}$ ratio commonly suggests that the $PM_{10}$ is more likely to be attributed to natural sources such as dust (Wang et al., 2015; Fan et al., 2021). Moreover, the NW and Central region are typical source areas of dust in China, therefore the increasing of $PM_{10}$ emissions over NW and Central regions may be mainly related to the enhanced dust emissions. This demonstrates the necessity to consider changes in natural emissions during COVID-19 restrictions. Thus, to reduce the effects of natural emissions on our findings, the same analysis was performed for the emissions over southeast China (Fig. S10) where emissions were dominated by anthropogenic sources, which shows consistent results with the findings above (Fig. S11 and Table S3).

### 3.2.3 Explanations for the emission changes during COVID-19 restrictions

Two explanations may help clarify the unbalanced emission changes between $NO_x$ and other species. First, the COVID-19 lockdown policy has led to dramatic decreases in transportation activities throughout China; however, as shown in Fig. 4, the relative contributions of the transportation sector to the emissions of $SO_2$ (2.4%), CO (18.5%), $PM_{2.5}$ (6.1%) and $PM_{10}$ (4.7%) are much smaller than those for $NO_x$ emissions (34.3%) (Zheng et al., 2018; Li et al., 2017a). Thus, the reduction in traffic activities can only substantially decrease $NO_x$ emissions. Reductions in CO emissions (-10.6%) were relatively larger than those for $SO_2$ (-9.7%) and $PM_{2.5}$ (-7.9%) emissions, which is consistent with the relatively larger contributions of the transportation sector to CO emissions. However, the differences in the percentage decreases in emissions of CO, $SO_2$ and $PM_{2.5}$ is not as significant as the differences in their transportation share (18% versus 2% and 6%). This may be on the one hand due to the uncertainty in the estimated relative contributions of different sectors to the total emissions of CO, $SO_2$ and $PM_{2.5}$, on the other hand were possibly due to the uncertainty in the emission inversions, especially considering that the decreasing trend of CO, $SO_2$ and $PM_{2.5}$ were not significant. Also, other factors beyond transportation may have influenced the reductions of anthropogenic emissions during P2 period. For example, the $PM_{10}$ emissions showed the largest reductions among these four species, which is related in part to the reduced dust emissions due to shutting down of construction sites during the lockdown period (Li et al., 2020). Second, as shown in Fig. 4, the industrial and residential sectors are the major contributors to the anthropogenic emissions of $SO_2$, CO, $PM_{2.5}$ and $PM_{10}$ in China, together contributing 77.6%, 78.3%, 86.5% and 86.3%, respectively, to their total emissions. The much smaller reductions of these species' emissions were thus in line with the fact that there were no intentional restrictions on heavy industry during the COVID-19 restrictions. A large number of non-interruptible processes, such as steel, glass, coke, refractory, petrochemical, electric power, and especially heating, cannot be stopped during the COVID-19 lockdown. According to statistical data from the National Bureau of Statistics of China (Fig. S12), the industrial and power sectors did not show similar reductions in their activity levels as those seen in the transportation sector. Power generation and steel production even showed increases in many provinces, which corresponds well with the emission increases over these regions. In addition, since people were required to stay at home, residential emissions were likely increased due to the increased energy consumption for heating or cooking. Therefore, our inversion results supported the views that the emissions of species related to industrial and residential activities did not decline much during the lockdown period, and that the COVID-19 lockdown policy was largely a traffic control measure with small influences on other sectors.

### 3.3 Investigation of air quality change over the NCP region during COVID-19 restrictions

Using the inversion results, we reassessed the environmental impacts of the COVID-19 restrictions on the air pollution over NCP region. The NCP region was chosen because it is the key target region of air pollution control in China and where unexpected severe haze occurred. A major caveat in previous studies that explored the impacts of COVID-19 lockdowns on air quality is the uncertainty in the emission changes during COVID-19 restrictions. The inversion results enable us give a more reliable assessment of the environmental impacts of COVID-19 restrictions. Figure 8 shows the observed changes in

PM$_{2.5}$ and O$_3$ concentrations over the NCP region from the P1 to P2 period. The observations showed consistent reductions in PM$_{2.5}$ concentrations over the NCP region (by 13.6 μg/m$^3$). However, substantial increases in PM$_{2.5}$ concentrations were observed in the Beijing area (by 31.2 μg/m$^3$). In contrast to the widespread reductions in PM$_{2.5}$ concentrations, the O$_3$ concentrations significantly increased over the whole NCP region (by 28.3 μg/m$^3$) and the Beijing area (by 16.8 μg/m$^3$). The simulations based on our inversion results reproduced the observed changes in PM$_{2.5}$ and O$_3$ concentrations over the NCP region well, although the O$_3$ concentrations were underestimated in all regions (Fig. S6) and the changes in PM$_{2.5}$ and O$_3$ concentrations were slightly overestimated by 1.6 and 2.6 μg/m$^3$ in the simulation (Fig. 8).

As detailed in the Sect 2.4, the simulated changes in air pollutant concentrations before and after lockdown were decomposed into meteorological-induced (MI) changes and emission-induced (EI) changes through two different scenarios to account for the nonlinearity of the atmospheric chemical system. According to Fig. S13, the differences in calculated MI and EI based on different scenarios were small for PM$_{2.5}$ concentrations, which were about 2 μg/m$^3$ in this application, while they were relatively larger for O$_3$, which were around 5 μg/m$^3$ over the Beijing and NCP region (Fig. S14). In addition, the sign of calculated MI using different scenarios were opposite although both suggested weak contributions of meteorological variation to the changes of O$_3$ concentrations. This suggests that the calculated MI and EI changes of O$_3$ concentrations could be more sensitive to the used scenarios, which may be associated with the stronger chemical nonlinearity of the O$_3$ concentrations. Figure 9 shows the mean results of the calculated MI and EI changes using the two different scenarios. It shows that the meteorological variation dominated the changes in PM$_{2.5}$ concentrations over the NCP region, which contributed 90% of the PM$_{2.5}$ reductions over most parts of the NCP region. Moreover, this variation made significant contributions (57.9%) to the increases in PM$_{2.5}$ concentrations over the Beijing area. This finding suggested that meteorological variations played an irreplaceable role in the occurrence of the unexpected PM$_{2.5}$ pollution around the Beijing area. Compared with the meteorological conditions before lockdown (Fig. 10), there were increases in relative humidity over northern China, which facilitated the reactions for aerosol formation and growth. Wind speed also decreased over the Beijing area accompanied by an anomalous south wind, which facilitated aerosol accumulation and the transportation of air pollutants from the polluted industrial regions of the Hebei Province to Beijing. The increases in boundary layer height from the P1 to P2 period were also much smaller in the Beijing area than in other areas of the NCP. Thus, the Beijing area has exhibited distinct meteorological variations from other areas of the NCP region, which correspond well to the different changes in PM$_{2.5}$ concentrations over the Beijing area.

The emission changes contributed slightly to the PM$_{2.5}$ reductions over the NCP region (8.6%). This is because, on the one hand, the large reductions in NO$_x$ emissions (by 44.4%) only reduced nitrate by approximately 10–30% due to the nonlinear effects of chemical reactions (Fig. 11), and on the other hand, the emissions of primary PM$_{2.5}$ and its precursors from other sectors changed little during the COVID-19 restrictions (Table 5). The emission changes contributed more to the increased PM$_{2.5}$ concentrations over the Beijing area (42.1%). This is mainly associated with the increases in primary PM$_{2.5}$ emissions around the Beijing area, as seen in Fig. 6, possibly due to the increased emissions from the industry as we mentioned before (Zuo et al., 2022) and the increased firework emissions during the Spring Festival as shown by the rapid increases in

13

concentrations of $K^+$ and $Mg^{2+}$ measured by CNEMC (Fig. S15). Therefore, our results suggested that the unexpected $PM_{2.5}$ pollution during lockdown period was mainly driven by unfavorable meteorological conditions together with small changes or even increases in primary $PM_{2.5}$ emissions. This finding is in line with previous results of Le et al. (2020) but different from those of Huang et al. (2021), who suggested that enhanced secondary aerosol formation was the main driver of severe haze during the COVID-19 restrictions. To investigate it, we further analyzed the changes in the concentrations of secondary inorganic aerosols (SIAs). First, we evaluated our model results against the observed SIA concentrations, which showed that the model results using our inversion emissions well reproduced the observed concentrations of SIAs over the NCP region (Fig. 12) with mean bias (MB) ranging from -5.14 to 5.45 $\mu g/m^3$ and correlation coefficient (R) ranging from 0.59 to 0.80. The observed increases in SIA concentrations over the Beijing area, especially for sulfate concentrations, were also captured in our simulations (Fig. 11), although underestimation occurred due to the uncertainty in simulating SIA concentrations. Through sensitivity experiments, we found that the increases in SIA concentrations were still driven by meteorological variations (Fig. 13). In fact, the emission reductions only led to a 10% decrease in SIA concentrations over the NCP region. This finding suggests that the enhanced secondary aerosol formation was likely mainly driven by the unfavorable meteorological conditions associated with higher temperature and relative humidity instead of the emission reductions during the lockdown period. This is in line with the observation evidences from Ma, T et al (2022) who emphasized that the increased temperature and relative humidity promoted the formation of secondary pollutants during the COVID-19 restrictions.

In terms of $O_3$ concentrations, the emission changes subsequently became the dominant contributor to the $O_3$ increases by more than 100% in the Beijing area and by 96.0% over the NCP region. This result is mainly because the lockdown period occurred in midwinter when photochemical $O_3$ formation was minimal; thus, the large increase in $O_3$ is expected solely from the effect of the reduced titration reaction associated with the large reductions in $NO_x$ emissions. Although the higher temperature and slower wind speed during the lockdown period were favorable for the increases in $O_3$ concentrations, their contributions were much smaller than those of emission changes (Fig. 9). These results suggested that control measures, such as COVID-19 restrictions, were inefficient for air pollution mitigation in China considering the high economic cost of the COVID-19 restrictions.

We also compared our results with previous studies that differentiated the contributions of meteorology and emission to the $PM_{2.5}$ and $O_3$ concentrations. Before comparisons, it should be noted that it is difficult to directly compare our results with previous studies due the altered definition of meteorological contribution, different reference period that used to quantify the meteorological contributions and different targeted region. For example, in Song et al. (2021), the reference period used to determine the meteorological contribution is the corresponding period of COVID-19 pandemic in 2019. Le et al. (2020) used the multiyear climatology as the reference period. In Wang et al. (2020) and Sulaymon et al. (2021), the MI changes of $PM_{2.5}$ concentrations were defined as the difference between the modeled concentrations in high-pollution days and those in low-pollution days under hypothetical emission reduction scenario. Zhao et al. (2020) used a similar reference period to ours to determine the MI changes but they used the outdated emission inventory. Table 6 summarized the results from the selected studies over Beijing and Beijing-Tianjin-Hebei region. Note that some studies only provided the relative changes in the

452 modeled PM$_{2.5}$ concentrations. It shows that due to the uncertainties in emission changes during COVID-19 pandemic, the EI

453 changes estimated by Zhao et al. (2020) were possibly overestimated compared to our studies (55% versus 24.7%). Both

454 Sulaymon et al. (2021) and Wang et al. (2020) suggested negative EI changes during COVID-19 period in Beijing. This

455 because they presumed that the emissions were largely reduced during COVID-19 lockdown which may deviate from the real

456 changes of emissions according to our inversion results. Meanwhile, although they used same method and reference period,

457 their results differed largely (-2.7 versus -13.4 $\mu g/m^3$) due to the different emission reduction scenario they assumed. Le et

458 al. (2020) only considered the emission reductions of NO$_x$ in their sensitivity simulations without considerations of other

459 species, therefore their calculated EI changes may be underestimated compared to our results (almost 0% versus 24.7%).

460 However, the calculated MI changes were consistent between our study and Le et al. (2020). In terms of O$_3$, the calculated EI

461 changes by our study were also higher than that calculated by Zhao et al. (2020) in Beijing (85.7% versus 70%). These results

462 suggested that the EI and MI changes calculated by our study could be more reasonable, considering that the emissions of

463 different species were well constrained which could better represent the temporal variation and spatial heterogeneity of

464 emission changes during COVID-19.

## 4 Conclusions and discussions

466 The COVID-19 pandemic is an unprecedented event that significantly influenced the social activity and associated

467 emissions of air pollutants. Our results provide a quantitative assessment of the influences of COVID-19 restrictions on multi-

468 air pollutant emissions in China. Otherwise, understanding of the relationship between air quality and human activities may

469 be biased. The inversion results provide important evidences that the COVID-19 lockdown policy was largely a traffic control

470 measure with substantially reducing impacts on NO$_x$ emissions but much smaller influences on the emissions of other species

471 and other sectors. Traffic control has widely been considered to be the normal protocol in implementing regulations in many

472 cities of China, but its effectiveness on air pollution control is still disputed (Han and Naeher, 2006; Zhang et al., 2007; Chen

473 et al., 2021; Cai and Xie, 2011; Chowdhury et al., 2017; Li et al., 2017c). Thus, the COVID-19 restrictions provided us with a

474 real nationwide traffic control scenario to investigate the effectiveness of traffic control on the mitigation of air pollution in

475 China. The results suggested that traffic control as a separate pollution control measure has limited effects on the coordinated

476 control of high concentrations of O$_3$ and PM$_{2.5}$ under the current air pollution conditions in China. In this case, the PM$_{2.5}$

477 concentrations were slightly reduced, while leading to substantial increases in O$_3$ concentrations. Severe haze was also not

478 avoided during the COVID-19 restrictions due to unbalanced emission changes from other sectors and unfavorable

479 meteorological conditions. China is now facing major challenges in both controlling PM$_{2.5}$ and controlling emerging O$_3$

480 pollution. The tragic COVID-19 pandemic has revealed the limitation of the road traffic control measure in the coordinated

481 control of PM$_{2.5}$ and O$_3$. More comprehensive regulations for multiple precursors from different sectors are required in the

482 future to address O$_3$ and PM$_{2.5}$ pollution in China.

483  Finally, there are certain limitations that should be aware of in our inversion work. Firstly, the COVID-19 restrictions
484 were initiated during the Spring Festival of China which would also influence the air pollutant emissions in China. However,
485 the inversion method used in this study did not differentiate the contributions of the Spring Festival from the COVID-19
486 restrictions. Similarly, the effects of natural emission changes were not differentiated in this study, which would lead to
487 uncertainty in quantifying the effects of the COVID-19 restrictions on air pollutant emissions. Secondly, the overestimations
488 of $NO_2$ measurement induced by chemiluminescence monitor interference were not directly corrected in our study due to the
489 lack of synchronous observations of $HNO_3$, PAN and AN, thus the estimated $NO_x$ emissions could be slightly overestimated
490 according to the sensitivity run with corrected $NO_2$ measurement using CFs (Fig. S16–18). Meanwhile, the sensitivity results
491 suggest that the inversed $NO_x$ emissions may even drop faster if the $NO_2$ measurement were corrected over the SE and SW
492 regions (Fig. S19). Thirdly, the use of outdated emission inventory as the a priori emission would also be a potential limitation
493 in our work although the iteration inversion method was used. A sensitivity inversion run was thus conducted based on the a
494 priori emission for a more recent year of 2018 to test the influence of the a priori emission inventory. This new emission
495 inventory is comprised of the anthropogenic emissions obtained from HTAPv3 (Crippa et al., 2023), the biogenic, soil and
496 oceanic emissions obtained from the CAMS global emission inventory
497 ([https://ads.atmosphere.copernicus.eu/cdsapp#!/dataset/cams-global-emission-inventories?tab=overview](https://ads.atmosphere.copernicus.eu/cdsapp#!/dataset/cams-global-emission-inventories?tab=overview), last access: March
498 15, 2023) and the biomass burning emissions obtained from the Global Fire Assimilation System (GFAS) (Kaiser et al., 2012).
499 Detailed steps of the new inversion estimation were same as those elucidated in Sect.2. The results suggest that the inversion
500 results based on the 2010 and 2018 inventory were broadly close to each other, while the inversion results based on 2018
501 inventory were relatively higher than those based on 2010 inventory, reflecting the uncertainty in our inversion results caused
502 by the choice of a priori emission inventory (Fig. S20–22). However, the sensitivity run consistently showed that the $NO_x$
503 emissions decreased much larger than other species (Fig. S23–24). This suggests that the choice of a priori emission inventory
504 may not obviously influence the main conclusion of our study, but can lead to uncertainty in the magnitude of the inversion
505 results which should be aware of by potential readers.

506

507

508

509

510

511

512

513

514

515

516

517 **Tables**

518 **Table 1. Corresponding relationship between the chemical observations and adjusted emissions**

| Species | Descriptions | Observations that used for inversions of this species |
|---|---|---|
| BC | black carbon | $PM_{2.5}$ |
| OC | organic carbon | $PM_{2.5}$ |
| PMF | fine mode unspeciated aerosol | $PM_{2.5}$ |
| PMC | coarse mode unspeciated aerosol | $PM_{10} - PM_{2.5}$ |
| $NO_x$ | nitrogen oxide | $NO_2$ |
| $SO_2$ | sulfur dioxide | $SO_2$ |
| CO | carbon monoxide | CO |

519

520 **Table 2. Configuration of simulation scenarios**

| Scenarios | Meteorology input | Emission input | Purpose |
|---|---|---|---|
| BASE scenario | varied meteorological condition from pre lockdown to lockdown period | varied emission from pre-lockdown to lockdown period | To estimate the total changes of air pollutant concentrations induced by emission and meteorological change |
| MET change scenario | varied meteorological condition from pre-lockdown to lockdown period | constant emissions during pre-lockdown and lockdown period | To estimate the impacts of meteorological changes on the air pollutants |
| EMIS change scenario | constant meteorological during pre-lockdown and lockdown period | varied emission from pre-lockdown to lockdown period | To estimate the impacts of emission changes on the air pollutants |

521
522
523
524
525
526
527

528

**Table 3. Descriptions of different items used in the calculation of meteorological-induced and emission-induced changes of air pollutant concentrations**

| notation | description |
|---|---|
| $MI$ | meteorological-induced changes in air pollutant concentrations |
| $EI$ | emission-induced changes in air pollutant concentrations |
| $MI_{MET\ change\ scenario}$ | meteorological-induced changes in air pollutant concentrations calculated by the MET change scenario |
| $EI_{MET\ change\ scenario}$ | emission-induced changes in air pollutant concentrations calculated by total changes minus $MI_{MET\ change\ scenario}$ |
| $EI_{EMIS\ change\ scenario}$ | emission-induced changes in air pollutant concentrations calculated by the EMIS change scenario |
| $MI_{EMIS\ change\ scenario}$ | meteorological-induced changes in air pollutant concentrations calculated by total changes minus $EI_{EMIS\ change\ scenario}$ |
| $conc_{p1,BASE\ scenario}$ | averaged concentrations of air pollutants during P1 period under the BASE scenario |
| $conc_{p2,BASE\ scenario}$ | averaged concentrations of air pollutants during P2 period under the BASE scenario |
| $conc_{p1,MET\ change\ scenario}$ | averaged concentrations of air pollutants during P1 period under the MET change scenario |
| $conc_{p2,MET\ change\ scenario}$ | averaged concentrations of air pollutants during P2 period under the MET change scenario |
| $conc_{p1,EMIS\ change\ scenario}$ | averaged concentrations of air pollutants during P1 period under the EMIS change scenario |
| $conc_{p2,EMIS\ change\ scenario}$ | averaged concentrations of air pollutants during P2 period under the EMIS change scenario |
| $contri_{met}$ | relative contributions of the meteorological variations to the changes in air pollutant concentrations |
| $contri_{emis}$ | relative contributions of the emission changes to the changes in air pollutant concentrations |

531

532

533

534

535

18

536 **Table 4. Inversion estimated emissions of different air pollutants in China and their changes between different periods during**
537 **COVID-19.**

|  | $NO_x$ | $SO_2$ | CO | $PM_{2.5}$ | $PM_{10}$ |
|---|---|---|---|---|---|
| P1 (Gg/day) | 72.9 | 23.8 | 1160.2 | 44.5 | 75.5 |
| P2 (Gg/day) | 41.9 | 21.5 | 1037.4 | 40.9 | 66.4 |
| P3 (Gg/day) | 44.8 | 23.2 | 1078.2 | 45.9 | 108.4 |
| (P2-P1)/P1 | -42.5% | -9.7% | -10.6% | -7.9% | -12.1% |
| (P3-P2)/P1 | 3.9% | 7.2% | 3.6% | 11.2% | 55.7% |
| (P3-P1)/P1 | -38.6% | -2.5% | -7.0% | 3.3% | 43.6% |

538
539
540
541
542
543
544
545
546
547
548
549
550
551
552
553
554
555
556
557
558
559
560

561  **Table 5. Inversion estimated emission changes of different air pollutants over different regions in China between different periods**
562  **during COVID-19 restrictions**

|  | $NO_x$ | $PM_{2.5}$ | $PM_{10}$ | $SO_2$ | CO |
|---|---|---|---|---|---|
| **NCP** | | | | | |
| (P2-P1)/P1 | -44.4% | 5.5% | 2.8% | -1.6% | -4.3% |
| (P3-P2)/P1 | -0.8% | -9.9% | 31.8% | -5.9% | -10.0% |
| (P3-P1)/P1 | -45.2% | -4.3% | 34.7% | -7.5% | -14.3% |
| **NE** | | | | | |
| (P2-P1)/P1 | -41.8% | -8.8% | -3.5% | -3.2% | -10.9% |
| (P3-P2)/P1 | -6.0% | -19.2% | 23.7% | -2.9% | -6.6% |
| (P3-P1)/P1 | -47.8% | -28.0% | 20.2% | -6.1% | -17.5% |
| **SE** | | | | | |
| (P2-P1)/P1 | -41.4% | -9.5% | -24.4% | -19.4% | -3.5% |
| (P3-P2)/P1 | 10.2% | 12.3% | 28.6% | 19.8% | 13.1% |
| (P3-P1)/P1 | -31.2% | 2.8% | 4.2% | 0.3% | 9.7% |
| **SW** | | | | | |
| (P2-P1)/P1 | -43.5% | -12.6% | -25.9% | -17.5% | -23.8% |
| (P3-P2)/P1 | 6.0% | 47.7% | 33.1% | 7.5% | 7.4% |
| (P3-P1)/P1 | -37.5% | 35.1% | 7.2% | -10.0% | -16.4% |
| **NW** | | | | | |
| (P2-P1)/P1 | -38.5% | -4.0% | -8.3% | 14.2% | -2.6% |
| (P3-P2)/P1 | -21.1% | 4.9% | 145.3% | -4.1% | -7.2% |
| (P3-P1)/P1 | -59.6% | 0.9% | 136.9% | 10.1% | -9.8% |
| **Central** | | | | | |
| (P2-P1)/P1 | -43.8% | -23.7% | -15.7% | -10.6% | -17.4% |
| (P3-P2)/P1 | 16.4% | 24.4% | 135.9% | 18.5% | 8.4% |
| (P3-P1)/P1 | -27.4% | 0.7% | 120.3% | 7.9% | -9.0% |

563

564

565

566  **Table 6. Calculated MI and EI changes in PM$_{2.5}$ concentrations during COVID-19 pandemic by previous studies**

|  | MI changes | EI changes | Region | Reference period | Method | Reference |
|---|---|---|---|---|---|---|
| 1 | 26.79 μg/m$^3$ | -21.84 μg/m$^3$ | Beijing | January 23-March 10, 2019 versus January 23-March 10, 2020 | observation-based wind-decomposition method | Song et al. (2021) |
| 2 | Around 20 μg/m$^3$ | -2.7 μg/m$^3$ | Beijing | January 01 to February 29, 2020 | CTM with hypothetical emission reduction scenario | Sulaymon et al. (2021) |
| 3 | Around 45 μg/m$^3$ | -13.4 μg/m$^3$ | Beijing | January 01 to February 29, 2020 | CTM with hypothetical emission reduction scenario | Wang et al. (2020) |
| 4 | 31.3% | Around 0% | Beijing-Tianjin-Hebei | January 01 to February 13, 2020 | CTM sensitivity simulations using different emission rates and multiyear climatology | Le et al. (2020) |
| 5 | Around 5% | Around 55% | Beijing | January 16-22, 2020 versus January 26 to February 1, 2020 | CTM with fixed emission inventory for 2017 | Zhao et al. (2020) |
| 6 | 17.5 μg/m$^3$ (34.0%) | 12.7 μg/m$^3$ (24.7%) | Beijing | January 1-20, 2020 versus January 21 to February 9, 2020 | CTM with inversion emission inventory | This study |

567

**Figures**



569
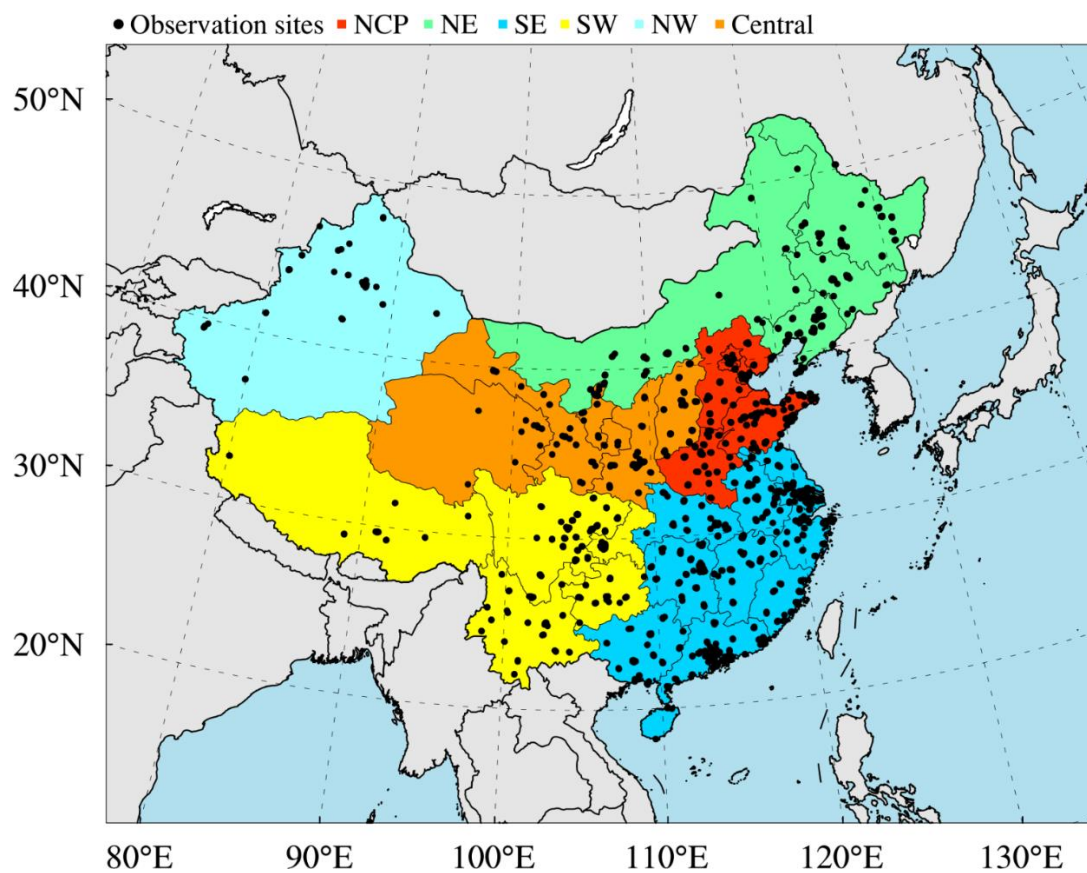
Figure 1: Modeling domain of the ensemble simulation overlay the distributions of observation sites from CNEMC. Different colours
denote the different regions in mainland of China, namely North China Plain (NCP), Northeast China (NE), Southwest China (SW),
Southeast China (SE), Northwest China (NW) and Central.
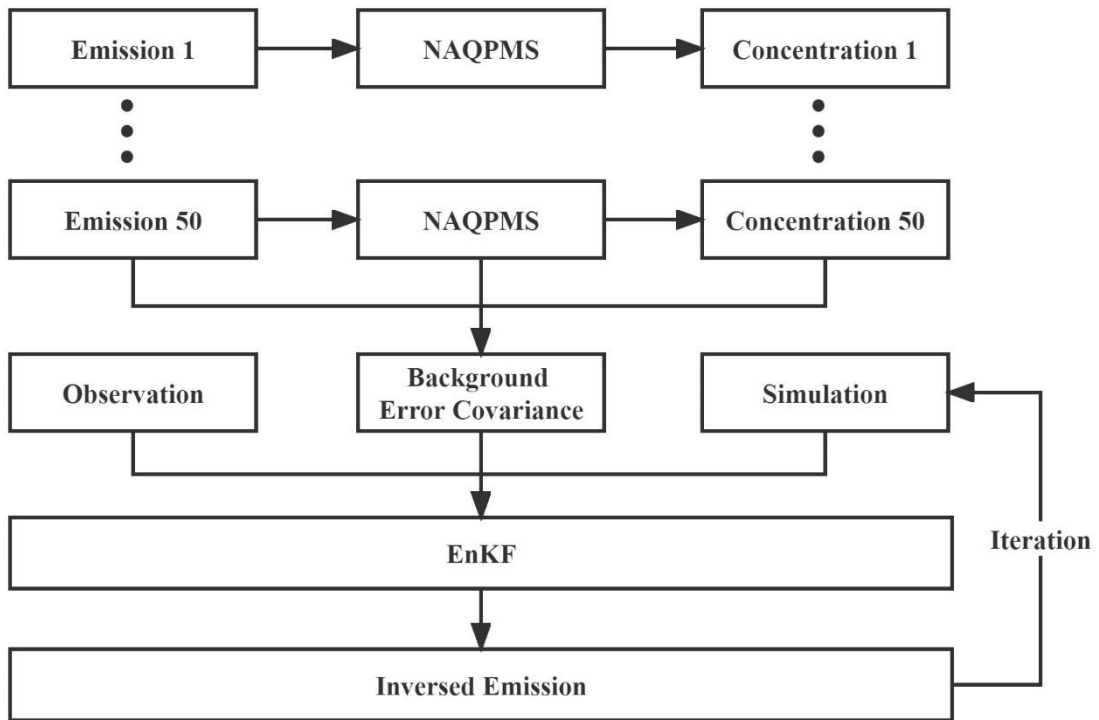
573

574    **Figure 2: Illustration of the iteration inversion scheme used in this study.**

575
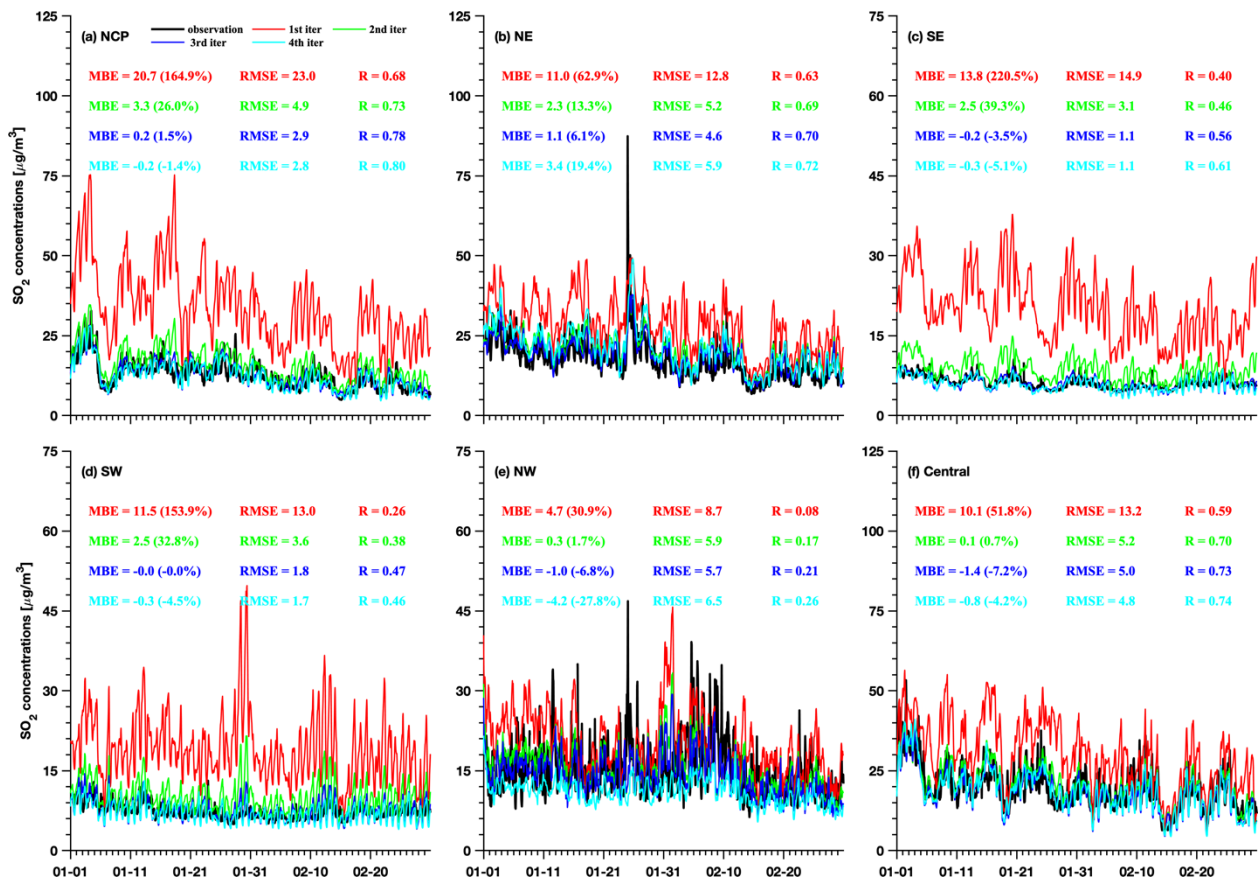
Figure 3: Comparisons of the observed and simulated mean SO₂ concentrations using emissions of different iteration time at validation sites over (a) NCP region, (b) NE region, (c) SE region, (d) SW region, (e) NW region and (f) Central region.
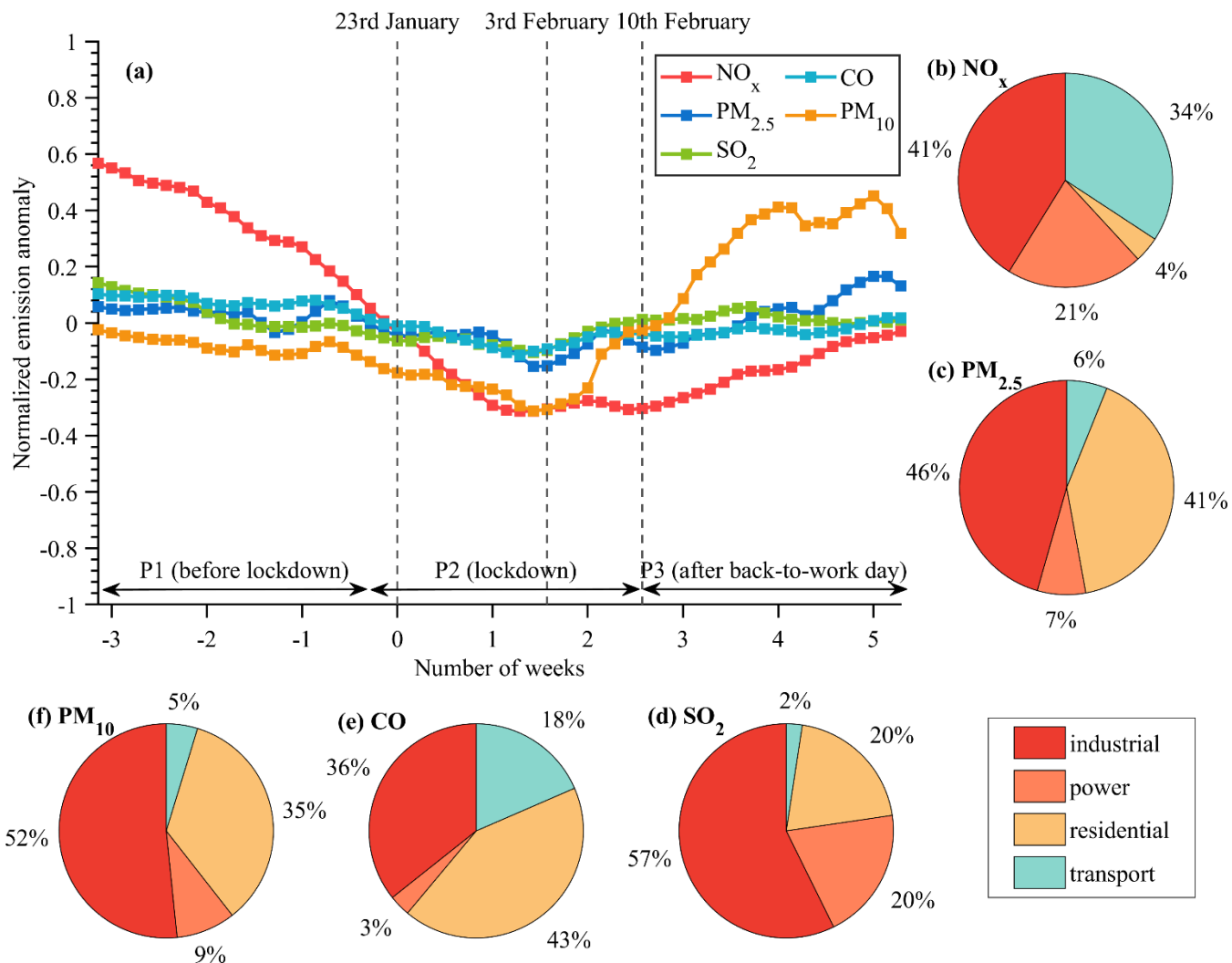
581
582
583 Figure 4: (a) Time series of normalized emission anomalies estimated by inversion results for different species in China from 1st
584 January to 29th February 2020, and (b-f) Relative contributions of different sectors to the total anthropogenic emissions of $NO_x$,
585 $PM_{2.5}$, $PM_{10}$, CO and $SO_2$ obtained from Zheng et al. (2018). The normalized emission anomaly is calculated by the emission anomaly
586 divided by the average emissions during the whole period.
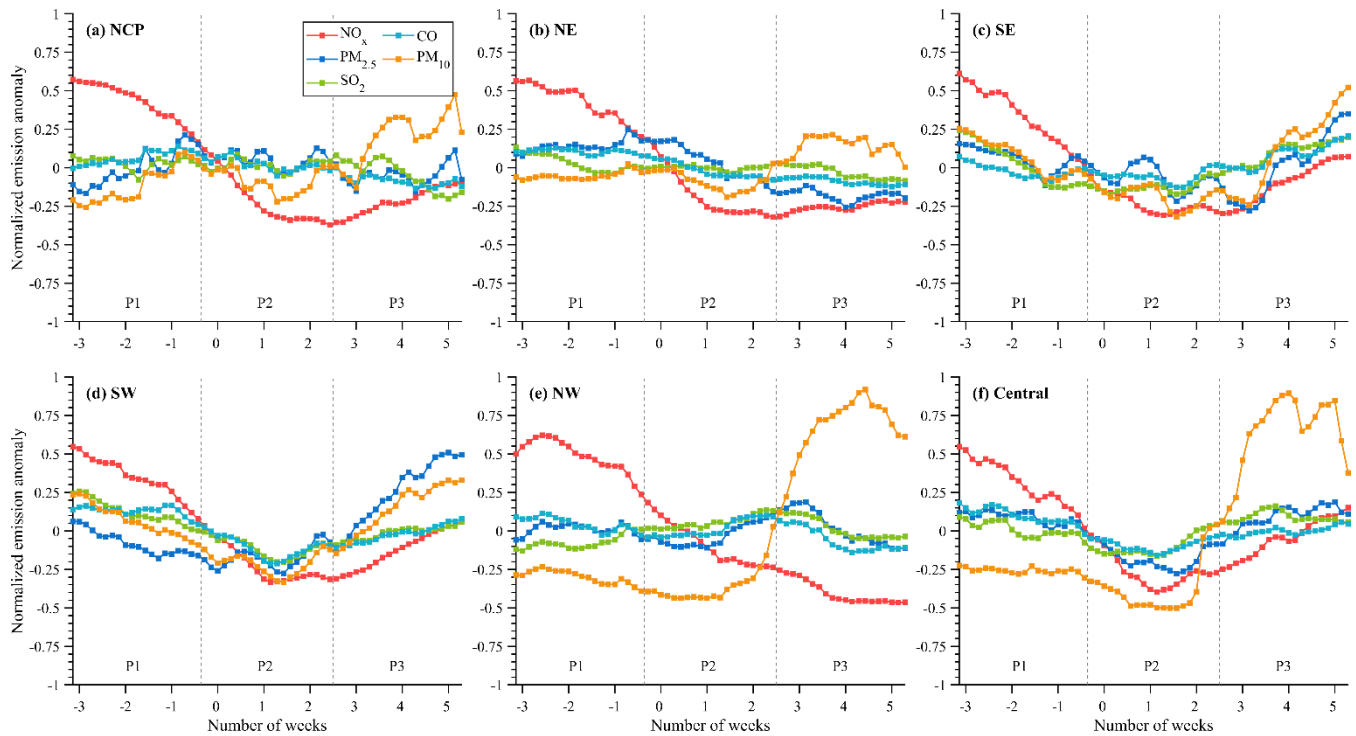
Figure 5: Time series of normalized emission anomalies estimated by inversion results for different species over (a) NCP region, (b) NE region, (c) SE region, (d) SW region, (e) NW region and (f) Central region from 1st January to 29th February 2020.
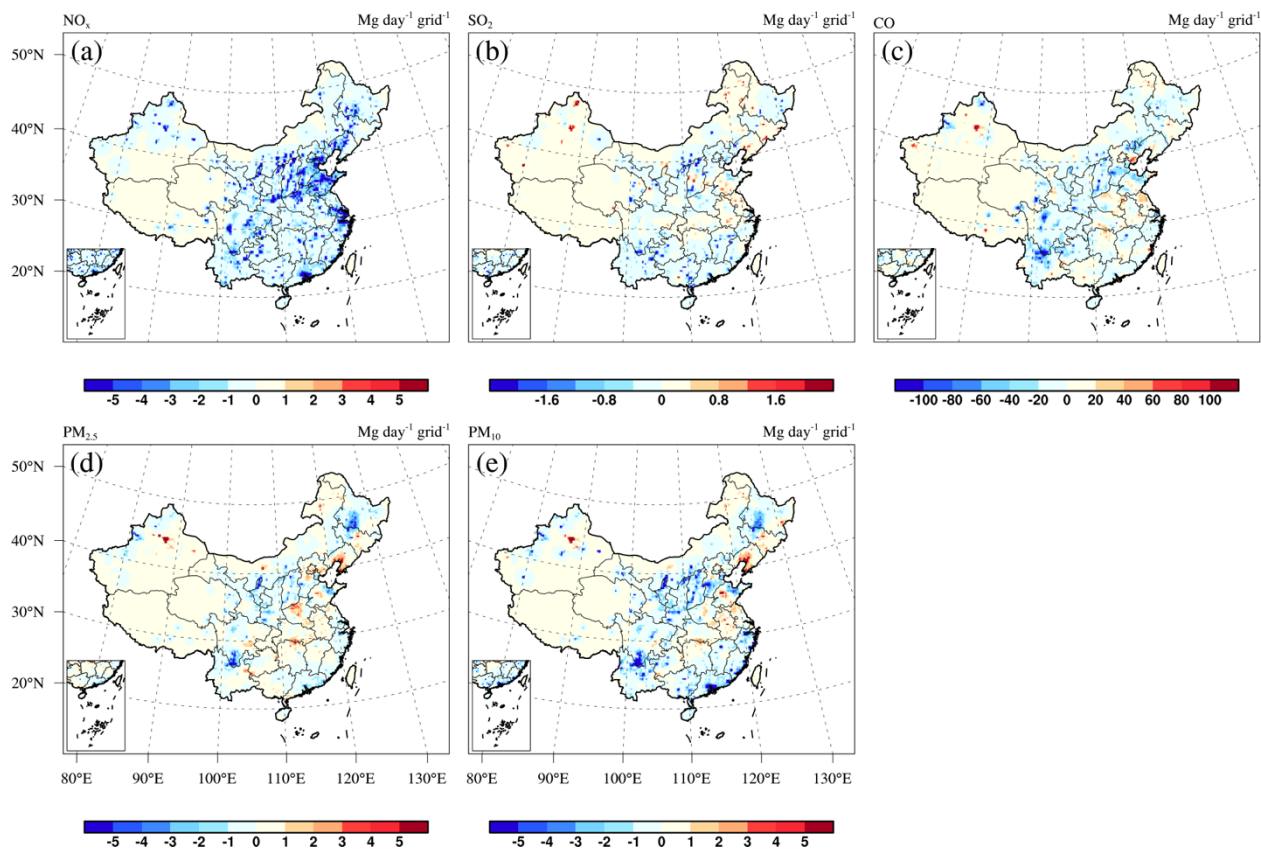
590

591　**Figure 6: The inversion estimated emission changes of (a) NO$_x$, (b) SO$_2$, (c) CO, (d) PM$_{2.5}$ and (e) PM$_{10}$ in China from P1 to P2 period.**
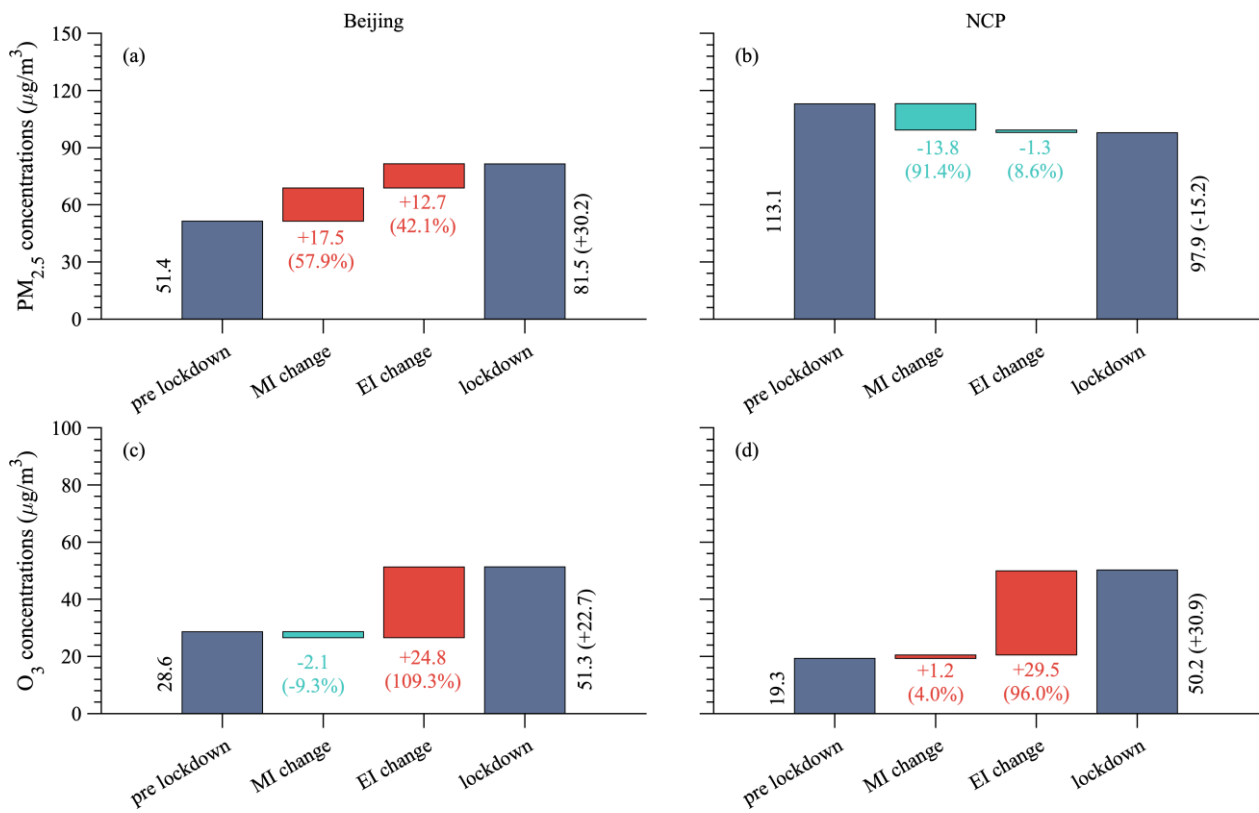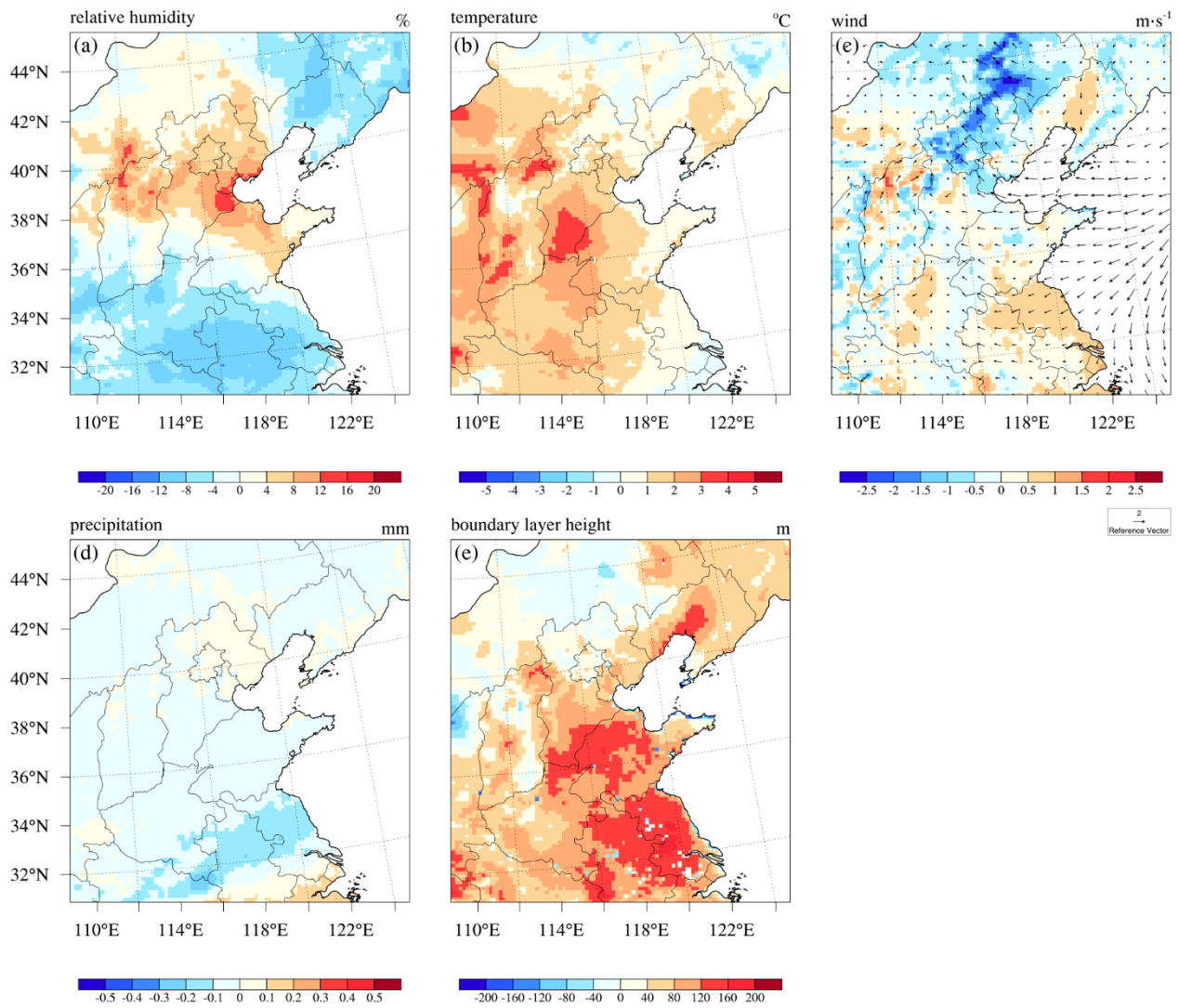
592
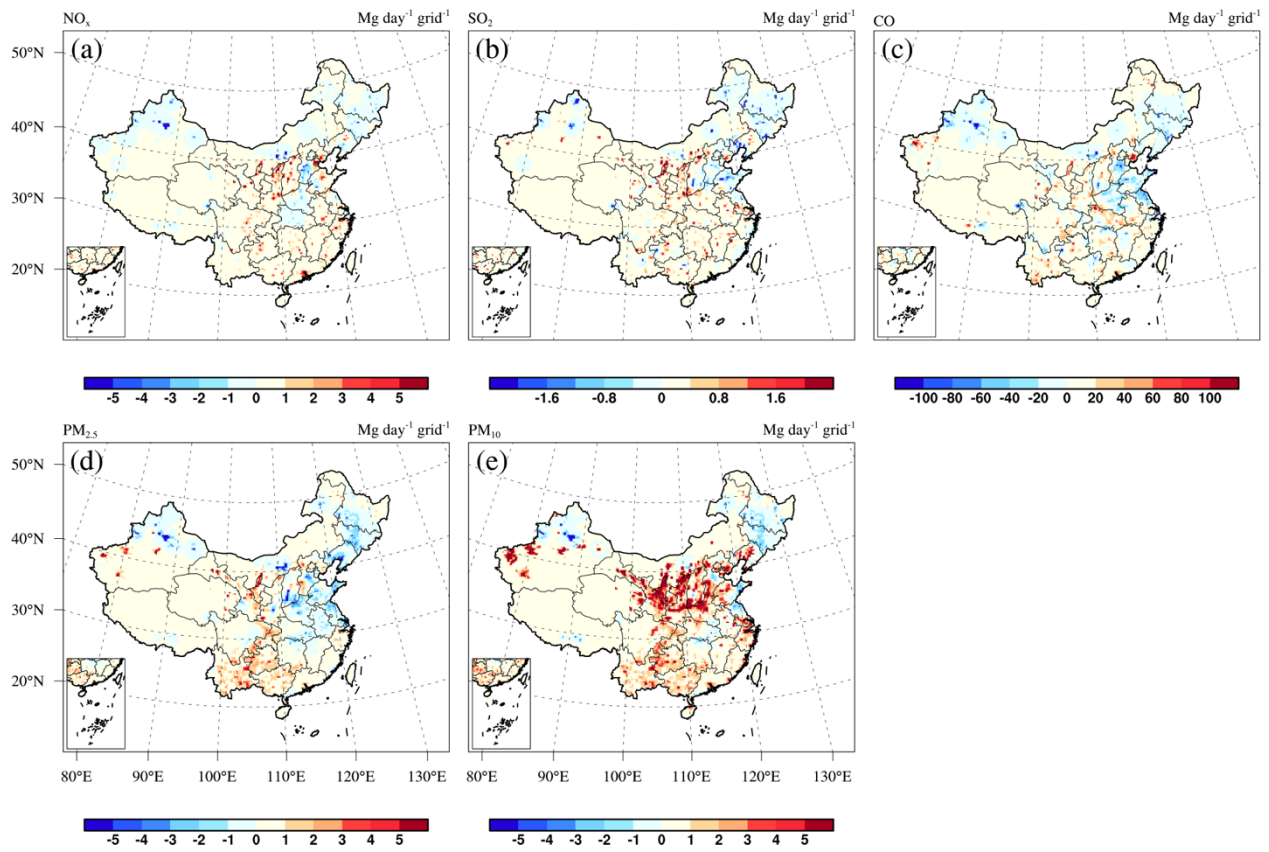
**Figure 7: The inversion estimated emission changes of (a) NO$_x$, (b) SO$_2$, (c) CO, (d) PM$_{2.5}$ and (e) PM$_{10}$ in China from P2 to P3 period.**

594

595
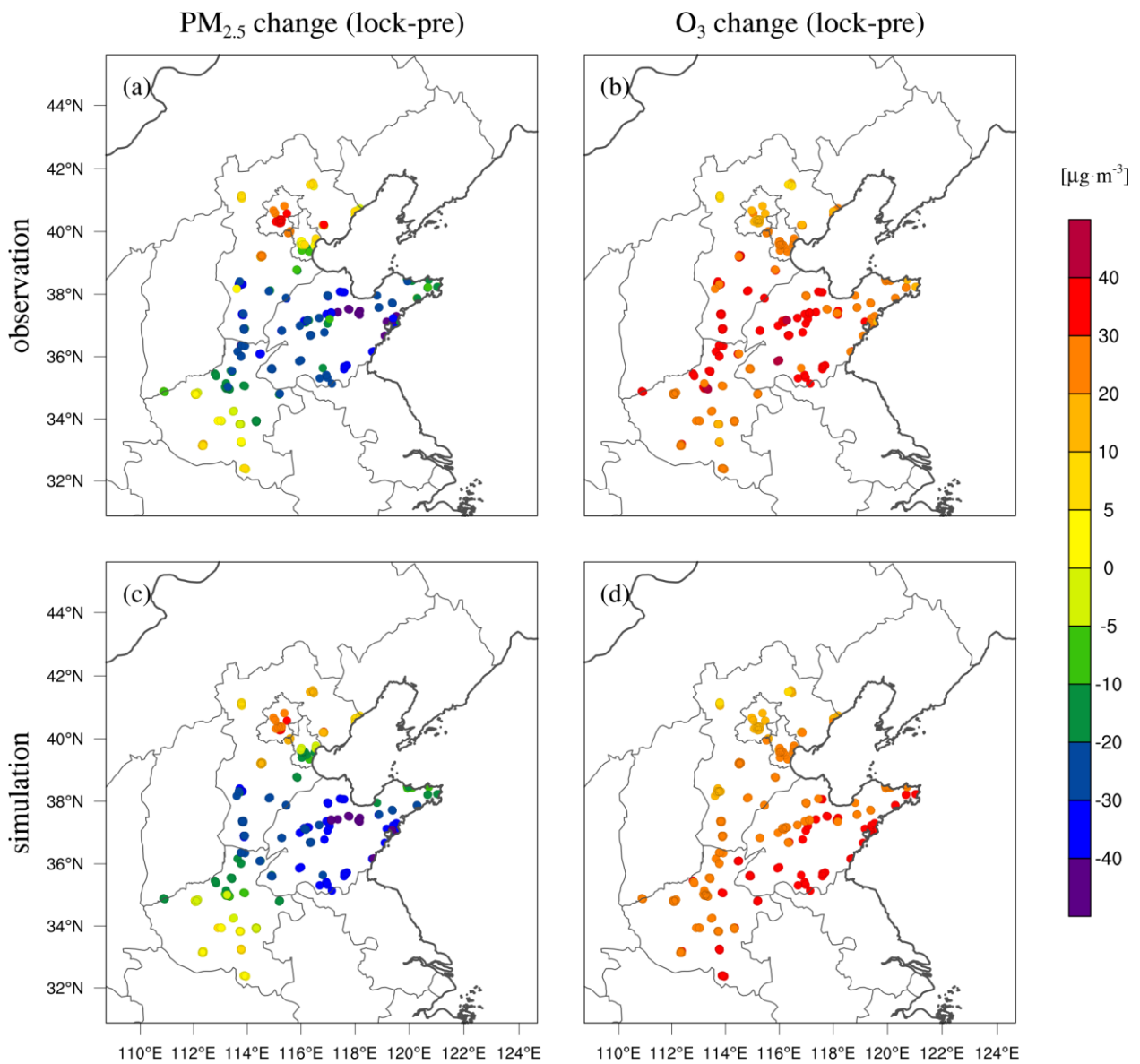
**Figure 8: Changes in the observed and simulated concentrations of (a, c) PM$_{2.5}$ and (b, d) O$_3$ over the NCP region from the pre lockdown period (P1) to the lockdown period (P2).**

Figure 9: Contributions of the meteorological variations and emission changes to the changes in (a, b) PM$_{2.5}$ and (c, d) O$_3$ concentrations over Beijing and the NCP region from the pre lockdown period (P1) to the lockdown period (P2).
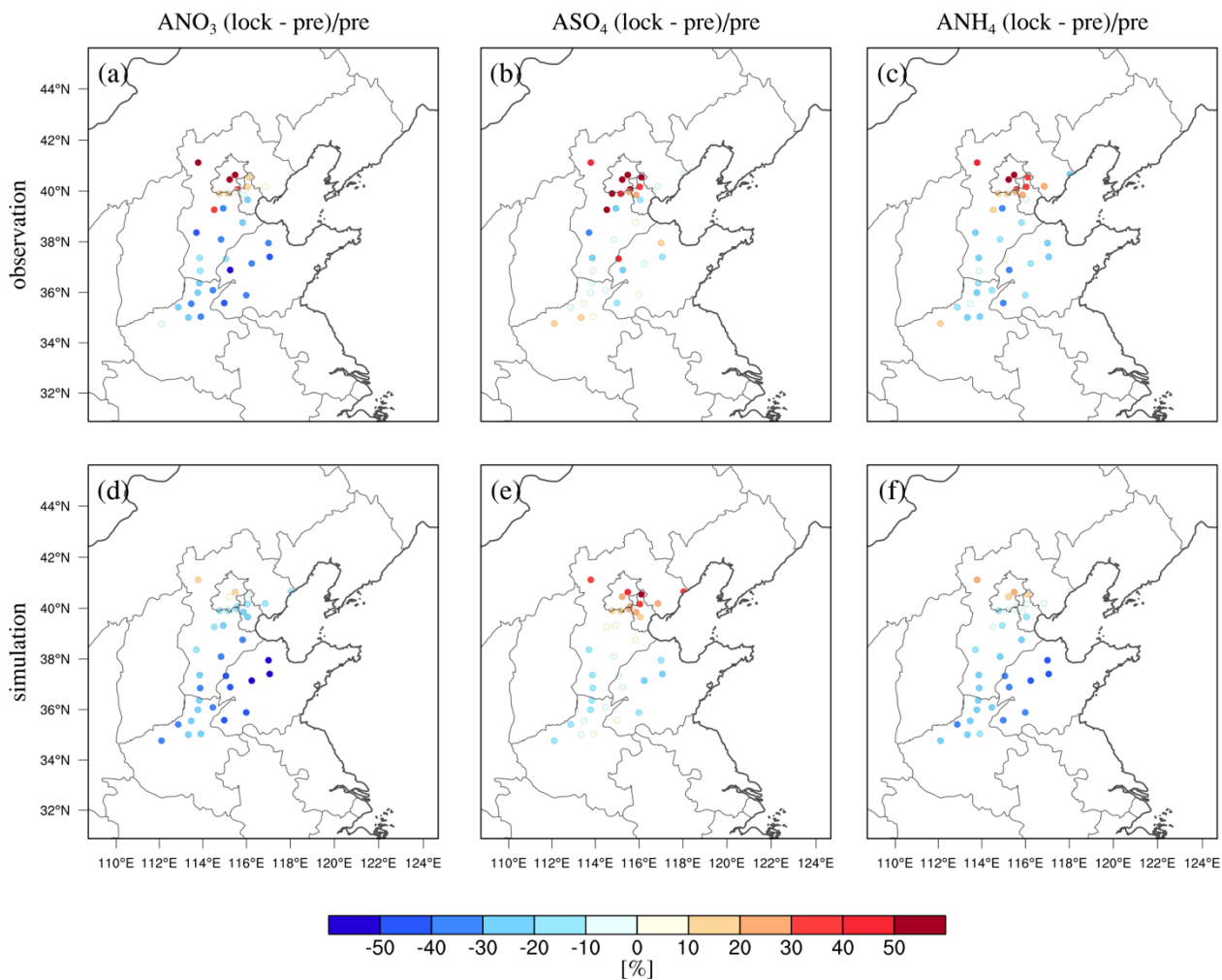
Figure 10: Changes in the (a) relative humidity, (b) temperature, (c) wind speed, (d) precipitation and (e) boundary layer height over the NCP region from P1 to P2 period obtained from WRF simulations.

608

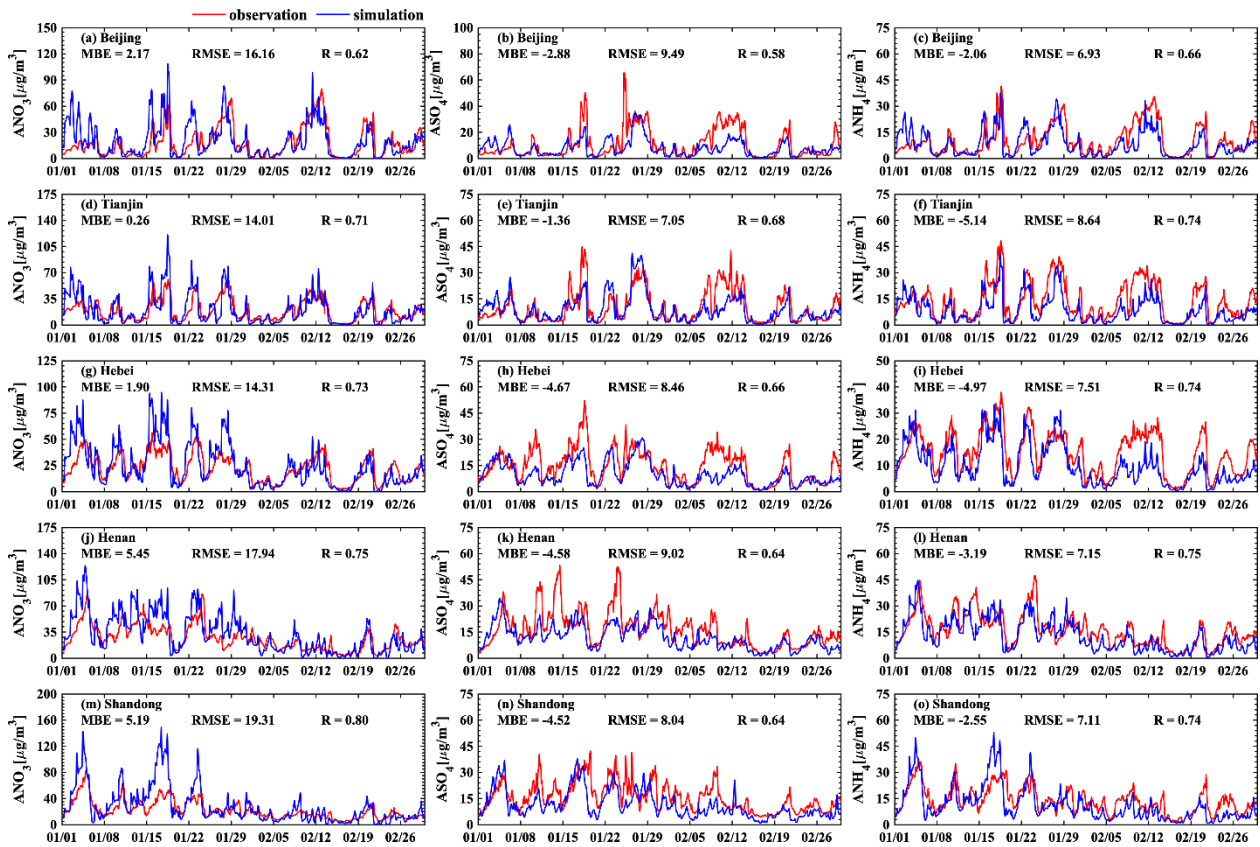**Figure 11: Relative changes in the simulated and observed concentrations of (a) ANO₃, (b) ASO₄, (c) ANH₄ over NCP region from P1 to P2 period.**
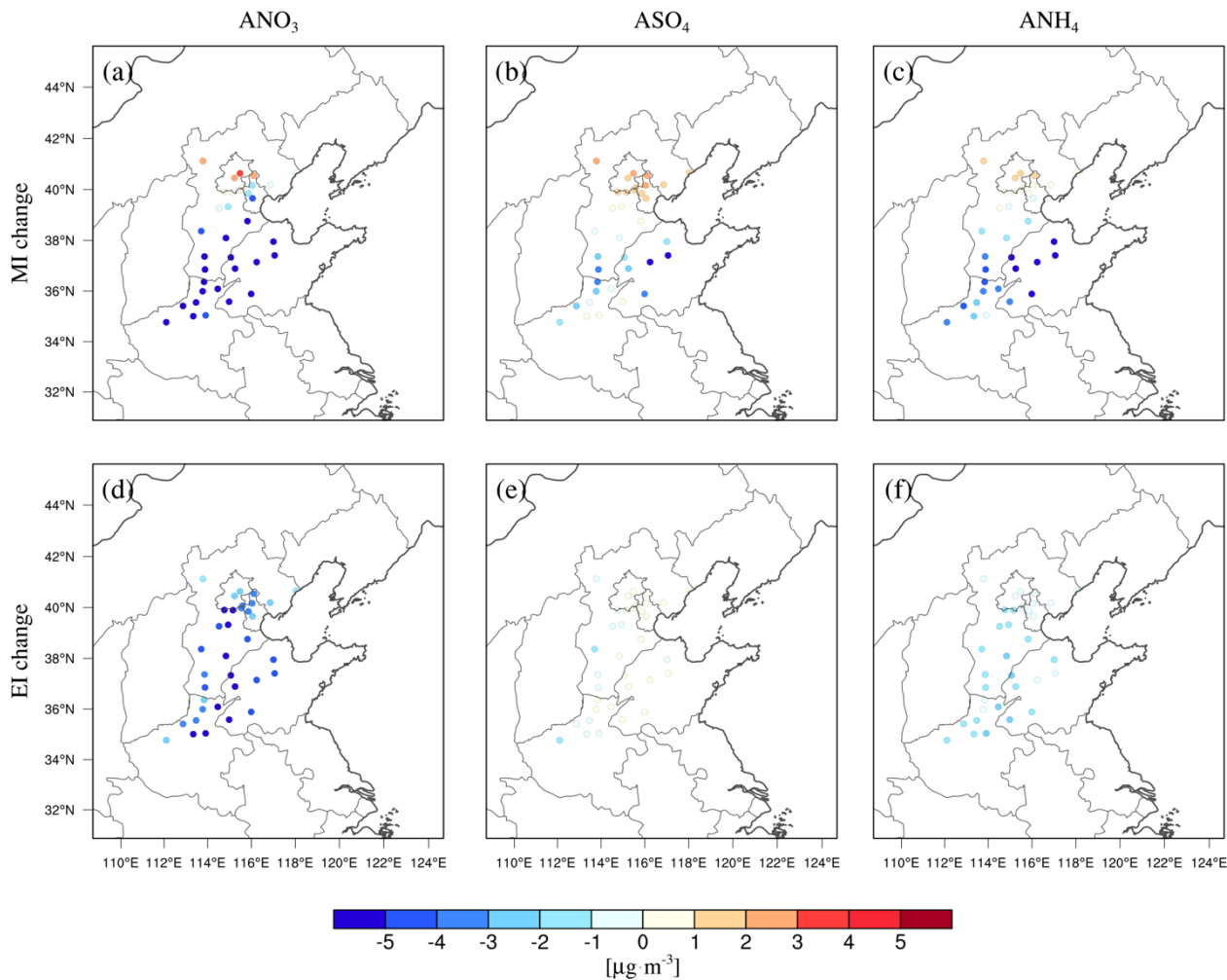
611

612

**Figure 12: Time series of observed and simulated concentrations of ANO₃, ASO₄ and ANH₄ in (a-c) Beijing, (b-f) Tianjin, (g-i) Heibei, (j-l) Henan and (m-o) Shangdong province from 1st January to 29th February 2020.**

615

616

**Figure 13: Meteorology-induced (MI) changes in the concentrations of (a) ANO$_3$, (b) ASO$_4$ and (c) ANH$_4$, as well as Emission-induced (EI) changes in the concentrations of (d) ANO$_3$, (e) ASO$_4$ and (f) ANH$_4$.**

**Data availability**

The hourly surface observations can be obtained from China National Environmental Monitoring Centre (http://www/cnemc.cn/en); The inversion estimated emissions of multi-air pollutants in China during COVID-19 lockdown period and the NAQPMS simulation results are available from the corresponding authors on request.

## Author contributions

X.T., J.Z., and Z.W. conceived and designed the project; H.W., L.K., X.T., and L.W. established the data assimilation system; M.L. Q.W. S.H. W.S. contributed to interpreting the data. L.K. conducted the inversion estimate, drew figures, and wrote the paper with comments provided by J.L., X.P., M.G., P.F., Y.S., H.A. and G.R.C.

## Competing interests

The authors declare no competing financial interest.

## Acknowledgements

## References

Brasseur, G. P., Hauglustaine, D. A., Walters, S., Rasch, P. J., Muller, J. F., Granier, C., and Tie, X. X.: MOZART, a global chemical transport model for ozone and related chemical tracers 1. Model description, J. Geophys. Res.-Atmos., 103, 28265-28289, https://doi.org/10.1029/98jd02397, 1998.

Cai, H. and Xie, S.: Traffic-related air pollution modeling during the 2008 Beijing Olympic Games: The effects of an odd-even day traffic restriction scheme, Sci. Total Environ., 409, 1935-1948, https://doi.org/10.1016/j.scitotenv.2011.01.025, 2011.

Chen, Z., Hao, X., Zhang, X., and Chen, F.: Have traffic restrictions improved air quality? A shock from COVID-19, J. Clean Prod., 279, 123622, https://doi.org/10.1016/j.jclepro.2020.123622, 2021.

Cheng, C., Barceló, J., Hartnett, A. S., Kubinec, R., and Messerschmidt, L.: COVID-19 Government Response Event Dataset (CoronaNet v.1.0), Nat. Hum. Behav., 4, 756-768, https://doi.org/10.1038/s41562-020-0909-7, 2020.

Chowdhury, S., Dey, S., Tripathi, S. N., Beig, G., Mishra, A. K., and Sharma, S.: "Traffic intervention" policy fails to mitigate air pollution in megacity Delhi, Environ. Sci. Policy, 74, 8-13, https://doi.org/10.1016/j.envsci.2017.04.018, 2017.

Chu, B., Zhang, S., Liu, J., Ma, Q., and He, H.: Significant concurrent decrease in PM2.5 and NO2 concentrations in China during COVID-19 epidemic, J. Environ. Sci., 99, 346-353, https://doi.org/10.1016/j.jes.2020.06.031, 2021.

Chu, K. K., Peng, Z., Liu, Z. Q., Lei, L. L., Kou, X. X., Zhang, Y., Bo, X., and Tian, J.: Evaluating the Impact of Emissions Regulations on the Emissions Reduction During the 2015 China Victory Day Parade With an Ensemble Square Root Filter, J. Geophys. Res.-Atmos., 123, 4122-4134, https://doi.org/10.1002/2017jd027631, 2018.

Cooper, M. J., Martin, R. V., McLinden, C. A., and Brook, J. R.: Inferring ground-level nitrogen dioxide concentrations at fine spatial resolution applied to the TROPOMI satellite instrument, Environ. Res. Lett., 15, 12, https://doi.org/10.1088/1748-9326/aba3a5, 2020.

655 Crippa, M., Guizzardi, D., Butler, T., Keating, T., Wu, R., Kaminski, J., Kuenen, J., Kurokawa, J., Chatani, S., Morikawa, T., Pouliot, G.,

656     Racine, J., Moran, M. D., Klimont, Z., Manseau, P. M., Mashayekhi, R., Henderson, B. H., Smith, S. J., Suchyta, H., Muntean, M., Solazzo,

657     E., Banja, M., Schaaf, E., Pagani, F., Woo, J. H., Kim, J., Monforti-Ferrario, F., Pisoni, E., Zhang, J., Niemi, D., Sassi, M., Ansari, T., and

658     Foley, K.: HTAP_v3 emission mosaic: a global effort to tackle air quality issues by quantifying global anthropogenic air pollutant sources,

659     Earth Syst. Sci. Data Discuss., 2023, 1-34, https://doi.org/10.5194/essd-2022-442, 2023.

660 Dai, Q., Liu, B., Bi, X., Wu, J., Liang, D., Zhang, Y., Feng, Y., and Hopke, P. K.: Dispersion Normalized PMF Provides Insights into the

661     Significant Changes in Source Contributions to PM2.5 after the COVID-19 Outbreak, Environ. Sci. Technol., 54, 9917-9927,

662     https://doi.org/10.1021/acs.est.0c02776, 2020.

663 Diamond, M. S. and Wood, R.: Limited Regional Aerosol and Cloud Microphysical Changes Despite Unprecedented Decline in Nitrogen

664     Oxide Pollution During the February 2020 COVID-19 Shutdown in China, Geophys. Res. Lett., 47, e2020GL088913,

665     https://doi.org/10.1029/2020gl088913, 2020.

666 Dunlea, E. J., Herndon, S. C., Nelson, D. D., Volkamer, R. M., San Martini, F., Sheehy, P. M., Zahniser, M. S., Shorter, J. H., Wormhoudt,

667     J. C., Lamb, B. K., Allwine, E. J., Gaffney, J. S., Marley, N. A., Grutter, M., Marquez, C., Blanco, S., Cardenas, B., Retama, A., Villegas,

668     C. R. R., Kolb, C. E., Molina, L. T., and Molina, M. J.: Evaluation of nitrogen dioxide chemiluminescence monitors in a polluted urban

669     environment, Atmos. Chem. Phys., 7, 2691-2704, https://doi.org/10.5194/acp-7-2691-2007, 2007.

670 Evensen, G.: Sequential data assimilation with a nonlinear quasi-geostrophic model using Monte Carlo methods to forecast error statistics, J.

671     Geophys. Res.-Oceans, 99, 10143-10162, https://doi.org/10.1029/94JC00572, 1994.

672 Fan, C., Li, Y., Guang, J., Li, Z. Q., Elnashar, A., Allam, M., and de Leeuw, G.: The Impact of the Control Measures during the COVID-19

673     Outbreak on Air Pollution in China, Remote Sens., 12, 23, https://doi.org/10.3390/rs12101613, 2020.

674 Fan, H., Zhao, C., Yang, Y., and Yang, X.: Spatio-Temporal Variations of the $PM_{2.5}/PM_{10}$ Ratios and Its Application to Air Pollution Type

675     Classification in China, Front. Environ. Sci., 9, https://doi.org/10.3389/fenvs.2021.692440, 2021.

676 Feng, S., Jiang, F., Wang, H., Wang, H., Ju, W., Shen, Y., Zheng, Y., Wu, Z., and Ding, A.: NOx Emission Changes Over China During the

677     COVID-19 Epidemic Inferred From Surface NO2 Observations, Geophys. Res. Lett., 47, e2020GL090080, 10.1029/2020gl090080, 2020.

678 Forster, P. M., Forster, H. I., Evans, M. J., Gidden, M. J., Jones, C. D., Keller, C. A., Lamboll, R. D., Le Quere, C., Rogelj, J., Rosen, D.,

679     Schleussner, C. F., Richardson, T. B., Smith, C. J., and Turnock, S. T.: Current and future global climate impacts resulting from COVID-

680     19, Nat. Clim. Chang., 10, 913-+, https://doi.org/10.1038/s41558-020-0883-0, 2020.

681 Granier, C., Lamarque, J., Mieville, A., Muller, J., Olivier, J., Orlando, J., Peters, J., Petron, G., Tyndall, G., and Wallens, S.: POET, a

682     database of surface emissions of ozone precursors, 2005.

683 Hammer, M. S., van Donkelaar, A., Martin, R. V., McDuffie, E. E., Lyapustin, A., Sayer, A. M., Hsu, N. C., Levy, R. C., Garay, M. J.,

684     Kalashnikova, O. V., and Kahn, R. A.: Effects of COVID-19 lockdowns on fine particulate matter concentrations, Sci. Adv., 7,

685     https://doi.org/10.1126/sciadv.abg7670, 2021.

686 Han, X. L. and Naeher, L. P.: A review of traffic-related air pollution exposure assessment studies in the developing world, Environ. Int., 32,

687     106-120, https://doi.org/10.1016/j.envint.2005.05.020, 2006.

688 Hauglustaine, D. A., Brasseur, G. P., Walters, S., Rasch, P. J., Muller, J. F., Emmons, L. K., and Carroll, C. A.: MOZART, a global chemical

689     transport model for ozone and related chemical tracers 2. Model results and evaluation, J. Geophys. Res.-Atmos., 103, 28291-28335,

690     https://doi.org/10.1029/98jd02398, 1998.

691 He, G. J., Pan, Y. H., and Tanaka, T.: The short-term impacts of COVID-19 lockdown on urban air pollution in China, Nat. Sustain., 3, 9,

692     https://doi.org/10.1038/s41893-020-0581-y, 2020.

693 He, T. L., Jones, D. B. A., Miyazaki, K., Bowman, K. W., Jiang, Z., Chen, X., Li, R., Zhang, Y., and Li, K.: Inverse modelling of Chinese
694     NOx emissions using deep learning: integrating in situ observations with a satellite-based chemical reanalysis, Atmos. Chem. Phys., 22,
695     14059-14074, https://doi.org/10.5194/acp-22-14059-2022, 2022.

696 Hu, Y., Zang, Z., Ma, X., Li, Y., Liang, Y., You, W., Pan, X., and Li, Z.: Four-dimensional variational assimilation for SO2 emission and its
697     application around the COVID-19 lockdown in the spring 2020 over China, Atmos. Chem. Phys., 22, 13183-13200,
698     https://doi.org/10.5194/acp-22-13183-2022, 2022.

699 Huang, X., Ding, A., Gao, J., Zheng, B., Zhou, D., Qi, X., Tang, R., Wang, J., Ren, C., Nie, W., Chi, X., Xu, Z., Chen, L., Li, Y., Che, F.,
700     Pang, N., Wang, H., Tong, D., Qin, W., Cheng, W., Liu, W., Fu, Q., Liu, B., Chai, F., Davis, S. J., Zhang, Q., and He, K.: Enhanced
701     secondary pollution offset reduction of primary emissions during COVID-19 lockdown in China, Natl. Sci. Rev., 8,
702     https://doi.org/10.1093/nsr/nwaa137, 2021.

703 Janssens-Maenhout, G., Crippa, M., Guizzardi, D., Dentener, F., Muntean, M., Pouliot, G., Keating, T., Zhang, Q., Kurokawa, J., Wankmuller,
704     R., van der Gon, H. D., Kuenen, J. J. P., Klimont, Z., Frost, G., Darras, S., Koffi, B., and Li, M.: HTAP_v2.2: a mosaic of regional and
705     global emission grid maps for 2008 and 2010 to study hemispheric transport of air pollution, Atmos. Chem. Phys., 15, 11411-11432,
706     https://doi.org/10.5194/acp-15-11411-2015, 2015.

707 Kaiser, J. W., Heil, A., Andreae, M. O., Benedetti, A., Chubarova, N., Jones, L., Morcrette, J. J., Razinger, M., Schultz, M. G., Suttie, M.,
708     and van der Werf, G. R.: Biomass burning emissions estimated with a global fire assimilation system based on observed fire radiative
709     power, Biogeosciences, 9, 527-554, https://doi.org/10.5194/bg-9-527-2012, 2012.

710 Kong, L., Tang, X., Zhu, J., Wang, Z., Pan, Y., Wu, H., Wu, L., Wu, Q., He, Y., Tian, S., Xie, Y., Liu, Z., Sui, W., Han, L., and Carmichael,
711     G.: Improved Inversion of Monthly Ammonia Emissions in China Based on the Chinese Ammonia Monitoring Network and Ensemble
712     Kalman Filter, Environ. Sci. Technol., 53, 12529-12538, https://doi.org/10.1021/acs.est.9b02701, 2019.

713 Kong, L., Tang, X., Zhu, J., Wang, Z., Li, J., Wu, H., Wu, Q., Chen, H., Zhu, L., Wang, W., Liu, B., Wang, Q., Chen, D., Pan, Y., Song, T.,
714     Li, F., Zheng, H., Jia, G., Lu, M., Wu, L., and Carmichael, G. R.: A 6-year-long (2013–2018) high-resolution air quality reanalysis dataset
715     in China based on the assimilation of surface observations from CNEMC, Earth Syst. Sci. Data, 13, 529-570, https://doi.org/10.5194/essd-
716     13-529-2021, 2021.

717 Lamsal, L. N., Martin, R. V., van Donkelaar, A., Steinbacher, M., Celarier, E. A., Bucsela, E., Dunlea, E. J., and Pinto, J. P.: Ground-level
718     nitrogen dioxide concentrations inferred from the satellite-borne Ozone Monitoring Instrument, J. Geophys. Res.-Atmos., 113,
719     https://doi.org/10.1029/2007JD009235, 2008.

720 Le, T. H., Wang, Y., Liu, L., Yang, J. N., Yung, Y. L., Li, G. H., and Seinfeld, J. H.: Unexpected air pollution with marked emission reductions
721     during the COVID-19 outbreak in China, Science, 369, 702-+, https://doi.org/10.1126/science.abb7431, 2020.

722 Levelt, P. F., Stein Zweers, D. C., Aben, I., Bauwens, M., Borsdorff, T., De Smedt, I., Eskes, H. J., Lerot, C., Loyola, D. G., Romahn, F.,
723     Stavrakou, T., Theys, N., Van Roozendael, M., Veefkind, J. P., and Verhoelst, T.: Air quality impacts of COVID-19 lockdown measures
724     detected from space using high spatial resolution observations of multiple trace gases from Sentinel-5P/TROPOMI, Atmos. Chem. Phys.,
725     22, https://doi.org/10319-10351, 10.5194/acp-22-10319-2022, 2022.

726 Li, B., Fan, J., Han, L., Sun, G., Zhang, D., and Zhang, P.: An Industrial Heat Source Extraction Method: BP Neural Network Using
727     Temperature Feature Template (in Chinese with English abstract), Journal of Geo-Information Science, 24, 533-545, 2022.

728 Li, F., Tang, X., Wang, Z., Zhu, L., Wang, X., Wu, H., Lu, M., Li, J., and Zhu, J.: Estimation of Representative Errors of Surface Observations
729     of Air Pollutant Concentrations Based on High-Density Observation Network over Beijing-Tianjin-Hebei Region, Chinese Journal of
730     Atmospheric Sciences, 43, 277-284, 2019.

731  Li, L., Li, Q., Huang, L., Wang, Q., Zhu, A., Xu, J., Liu, Z., Li, H., Shi, L., Li, R., Azari, M., Wang, Y., Zhang, X., Liu, Z., Zhu, Y., Zhang,
732      K., Xue, S., Ooi, M. C. G., Zhang, D., and Chan, A.: Air quality changes during the COVID-19 lockdown over the Yangtze River Delta
733      Region: An insight into the impact of human activity pattern changes on air pollution variation, Sci. Total Environ., 732, 139282,
734      https://doi.org/10.1016/j.scitotenv.2020.139282, 2020.

735  Li, M., Wang, T., Xie, M., Li, S., Zhuang, B., Fu, Q., Zhao, M., Wu, H., Liu, J., Saikawa, E., and Liao, K.: Drivers for the poor air quality
736      conditions in North China Plain during the COVID-19 outbreak, Atmos. Environ., 246, 118103,
737      https://doi.org/10.1016/j.atmosenv.2020.118103, 2021.

738  Li, M., Liu, H., Geng, G. N., Hong, C. P., Liu, F., Song, Y., Tong, D., Zheng, B., Cui, H. Y., Man, H. Y., Zhang, Q., and He, K. B.:
739      Anthropogenic emission inventories in China: a review, Natl. Sci. Rev., 4, 834-866, https://doi.org/10.1093/nsr/nwx150, 2017a.

740  Li, M., Zhang, Q., Kurokawa, J. I., Woo, J. H., He, K., Lu, Z., Ohara, T., Song, Y., Streets, D. G., Carmichael, G. R., Cheng, Y., Hong, C.,
741      Huo, H., Jiang, X., Kang, S., Liu, F., Su, H., and Zheng, B.: MIX: a mosaic Asian anthropogenic emission inventory under the international
742      collaboration framework of the MICS-Asia and HTAP, Atmos. Chem. Phys., 17, 935-963, https://doi.org/10.5194/acp-17-935-2017, 2017b.

743  Li, M., Zhang, Q., Zheng, B., Tong, D., Lei, Y., Liu, F., Hong, C. P., Kang, S. C., Yan, L., Zhang, Y. X., Bo, Y., Su, H., Cheng, Y. F., and
744      He, K. B.: Persistent growth of anthropogenic non-methane volatile organic compound (NMVOC) emissions in China during 1990-2017:
745      drivers, speciation and ozone formation potential, Atmos. Chem. Phys., 19, 8897-8913, https://doi.org/10.5194/acp-19-8897-2019, 2019.

746  Li, X., Zhang, Q., Zhang, Y., Zhang, L., Wang, Y. X., Zhang, Q. Q., Li, M., Zheng, Y. X., Geng, G. N., Wallington, T. J., Han, W. J., Shen,
747      W., and He, K. B.: Attribution of PM2.5 exposure in Beijing-Tianjin-Hebei region to emissions: implication to control strategies, Sci.
748      Bull., 62, 957-964, https://doi.org/10.1016/j.scib.2017.06.005, 2017c.

749  Ma, C. Q., Wang, T. J., Mizzi, A. P., Anderson, J. L., Zhuang, B. L., Xie, M., and Wu, R. S.: Multiconstituent Data Assimilation With WRF-
750      Chem/DART: Potential for Adjusting Anthropogenic Emissions and Improving Air Quality Forecasts Over Eastern China, J. Geophys.
751      Res.-Atmos., 124, 7393-7412, https://doi.org/10.1029/2019jd030421, 2019.

752  Ma, T., Duan, F. K., Ma, Y. L., Zhang, Q. Q., Xu, Y. Z., Li, W. G., Zhu, L. D., and He, K. B.: Unbalanced emission reductions and adverse
753      meteorological conditions facilitate the formation of secondary pollutants during the COVID-19 lockdown in Beijing, Sci. Total Environ.,
754      838, 8, https://doi.org/10.1016/j.scitotenv.2022.155970, 2022.

755  Miyazaki, K., Eskes, H. J., Sudo, K., Takigawa, M., van Weele, M., and Boersma, K. F.: Simultaneous assimilation of satellite NO2, O-3,
756      CO, and HNO3 data for the analysis of tropospheric chemical composition and emissions, Atmos. Chem. Phys., 12, 9545-9579,
757      https://doi.org/10.5194/acp-12-9545-2012, 2012.

758  Okuda, T., Matsuura, S., Yamaguchi, D., Umemura, T., Hanada, E., Orihara, H., Tanaka, S., He, K., Ma, Y., Cheng, Y., and Liang, L.: The
759      impact of the pollution control measures for the 2008 Beijing Olympic Games on the chemical composition of aerosols, Atmos. Environ.,
760      45, 2789-2794, https://doi.org/10.1016/j.atmosenv.2011.01.053, 2011.

761  Peng, Z., Lei, L. L., Liu, Z. Q., Su, J. N., Ding, A. J., Ban, J. M., Chen, D., Kou, X. X., and Chu, K. K.: The impact of multi-species surface
762      chemical observation assimilation on air quality forecasts in China, Atmos. Chem. Phys., 18, 18, https://doi.org/10.5194/acp-18-17387-
763      2018, 2018.

764  Price, C., Penner, J., and Prather, M.: NOx from lightning .1. Global distribution based on lightning physics, J. Geophys. Res.-Atmos., 102,
765      5929-5941, https://doi.org/10.1029/96jd03504, 1997.

766  Randerson, J. T., Van Der Werf, G. R., Giglio, L., Collatz, G. J., and Kasibhatla, P. S.: Global Fire Emissions Database, Version 4.1 (GFEDv4),
767      10.3334/ornldaac/1293, 2017.

Sakov, P. and Oke, P. R.: A deterministic formulation of the ensemble Kalman filter: an alternative to ensemble square root filters, Tellus Ser. A-Dyn. Meteorol. Oceanol., 60, 361-371, https://doi.org/10.1111/j.1600-0870.2007.00299.x, 2008.

Skachko, S., Errera, Q., Ménard, R., Christophe, Y., and Chabrillat, S.: Comparison of the ensemble Kalman filter and 4D-Var assimilation methods using a stratospheric tracer transport model, Geosci. Model Dev., 7, 1451-1465, https://doi.org/10.5194/gmd-7-1451-2014, 2014.

Shi, X. and Brasseur, G. P.: The Response in Air Quality to the Reduction of Chinese Economic Activities During the COVID-19 Outbreak, Geophys. Res. Lett., 47, e2020GL088070, https://doi.org/10.1029/2020gl088070, 2020.

Shi, Z., Song, C., Liu, B., Lu, G., Xu, J., Van Vu, T., Elliott, R. J. R., Li, W., Bloss, W. J., and Harrison, R. M.: Abrupt but smaller than expected changes in surface air quality attributable to COVID-19 lockdowns, Sci. Adv., 7, eabd6696, https://doi.org/10.1126/sciadv.abd6696, 2021.

Sindelarova, K., Granier, C., Bouarar, I., Guenther, A., Tilmes, S., Stavrakou, T., Muller, J. F., Kuhn, U., Stefani, P., and Knorr, W.: Global data set of biogenic VOC emissions calculated by the MEGAN model over the last 30 years, Atmos. Chem. Phys., 14, 9317-9341, https://doi.org/10.5194/acp-14-9317-2014, 2014.

Skamarock, W. C.: A description of the advanced research WRF version 3, Ncar Technical, 113, 7-25, 2008.

Song, Y. S., Lin, C. Q., Li, Y., Lau, A. K. H., Fung, J. C. H., Lu, X. C., Guo, C., Ma, J., and Lao, X. Q.: An improved decomposition method to differentiate meteorological and anthropogenic effects on air pollution: A national study in China during the COVID-19 lockdown period, Atmos. Environ., 250, 9, https://doi.org/10.1016/j.atmosenv.2021.118270, 2021.

Streets, D. G., Bond, T. C., Carmichael, G. R., Fernandes, S. D., Fu, Q., He, D., Klimont, Z., Nelson, S. M., Tsai, N. Y., Wang, M. Q., Woo, J. H., and Yarber, K. F.: An inventory of gaseous and primary aerosol emissions in Asia in the year 2000, J. Geophys. Res.-Atmos., 108, 23, https://doi.org/10.1029/2002JD003093, 2003.

Streets, D. G., Canty, T., Carmichael, G. R., de Foy, B., Dickerson, R. R., Duncan, B. N., Edwards, D. P., Haynes, J. A., Henze, D. K., Houyoux, M. R., Jacob, D. J., Krotkov, N. A., Lamsal, L. N., Liu, Y., Lu, Z., Martin, R. V., Pfister, G. G., Pinder, R. W., Salawitch, R. J., and Wecht, K. J.: Emissions estimation from satellite retrievals: A review of current capability, Atmos. Environ., 77, 1011-1042, https://doi.org/10.1016/j.atmosenv.2013.05.051, 2013.

Sulaymon, I. D., Zhang, Y., Hopke, P. K., Hu, J., Zhang, Y., Li, L., Mei, X., Gong, K., Shi, Z., Zhao, B., and Zhao, F.: Persistent high PM2.5 pollution driven by unfavorable meteorological conditions during the COVID-19 lockdown period in the Beijing-Tianjin-Hebei region, China, Environ. Res., 198, 111186, https://doi.org/10.1016/j.envres.2021.111186, 2021.

Tandeo, P., Ailliot, P., Bocquet, M., Carrassi, A., Miyoshi, T., Pulido, M., and Zhen, Y. C.: A Review of Innovation-Based Methods to Jointly Estimate Model and Observation Error Covariance Matrices in Ensemble Data Assimilation, Mon. Weather Rev., 148, 3973-3994, https://doi.org/10.1175/mwr-d-19-0240.1, 2020.

Tang, G., Zhu, X., Hu, B., Xin, J., Wang, L., Münkel, C., Mao, G., and Wang, Y.: Impact of emission controls on air quality in Beijing during APEC 2014: lidar ceilometer observations, Atmos. Chem. Phys., 15, 12667-12680, https://doi.org/10.5194/acp-15-12667-2015, 2015.

Tang, X., Zhu, J., Wang, Z. F., and Gbaguidi, A.: Improvement of ozone forecast over Beijing based on ensemble Kalman filter with simultaneous adjustment of initial conditions and emissions, Atmos. Chem. Phys., 11, 12901-12916, 10.5194/acp-11-12901-2011, 2011.

Tang, X., Zhu, J., Wang, Z. F., Wang, M., Gbaguidi, A., Li, J., Shao, M., Tang, G. Q., and Ji, D. S.: Inversion of CO emissions over Beijing and its surrounding areas with ensemble Kalman filter, Atmos. Environ., 81, 676-686, https://doi.org/10.1016/j.atmosenv.2013.08.051, 2013.

804 van der Werf, G. R., Randerson, J. T., Giglio, L., Collatz, G. J., Mu, M., Kasibhatla, P. S., Morton, D. C., DeFries, R. S., Jin, Y., and van

805 Leeuwen, T. T.: Global fire emissions and the contribution of deforestation, savanna, forest, agricultural, and peat fires (1997–2009),

806 Atmos. Chem. Phys., 10, 11707-11735, https://doi.org/10.5194/acp-10-11707-2010, 2010.

807 Wang, P., Chen, K., Zhu, S., Wang, P., and Zhang, H.: Severe air pollution events not avoided by reduced anthropogenic activities during

808 COVID-19 outbreak, Resour. Conserv. Recycl., 158, 104814, https://doi.org/10.1016/j.resconrec.2020.104814, 2020.

809 Wang, S., Gao, J., Zhang, Y., Zhang, J., Cha, F., Wang, T., Ren, C., and Wang, W.: Impact of emission control on regional air quality: An

810 observational study of air pollutants before, during and after the Beijing Olympic Games, J. Environ. Sci., 26, 175-180,

811 https://doi.org/10.1016/S1001-0742(13)60395-2, 2014.

812 Wang, Y. Q., Zhang, X. Y., Sun, J. Y., Zhang, X. C., Che, H. Z., and Li, Y.: Spatial and temporal variations of the concentrations of $PM_{10}$,

813 $PM_{2.5}$ and $PM_1$ in China, Atmos. Chem. Phys., 15, 13585-13598, https://doi.org/10.5194/acp-15-13585-2015, 2015.

814 Wang, Z., Uno, I., Yumimoto, K., Itahashi, S., Chen, X., Yang, W., and Wang, Z.: Impacts of COVID-19 lockdown, Spring Festival and

815 meteorology on the NO2 variations in early 2020 over China based on in-situ observations, satellite retrievals and model simulations,

816 Atmos. Environ., 244, 117972, https://doi.org/10.1016/j.atmosenv.2020.117972, 2021.

817 Wu, H., Tang, X., Wang, Z., Wu, L., Li, J., Wang, W., Yang, W., and Zhu, J.: High-spatiotemporal-resolution inverse estimation of CO and

818 NOx emission reductions during emission control periods with a modified ensemble Kalman filter, Atmos. Environ., 236, 117631,

819 https://doi.org/10.1016/j.atmosenv.2020.117631, 2020.

820 Wu, H. J., Tang, X., Wang, Z. F., Wu, L., Lu, M. M., Wei, L. F., and Zhu, J.: Probabilistic Automatic Outlier Detection for Surface Air

821 Quality Measurements from the China National Environmental Monitoring Network, Adv. Atmos. Sci., 35, 1522-1532,

822 https://doi.org/10.1007/s00376-018-8067-9, 2018.

823 Xing, J., Li, S. W., Jiang, Y. Q., Wang, S. X., Ding, D., Dong, Z. X., Zhu, Y., and Hao, J. M.: Quantifying the emission changes and associated

824 air quality impacts during the COVID-19 pandemic on the North China Plain: a response modeling study, Atmos. Chem. Phys., 20, 14347-

825 14359, https://doi.org/10.5194/acp-20-14347-2020, 2020.

826 Yan, C., Shen, Y. C., Stolzenburg, D., Dada, L., Qi, X. M., Hakala, S., Sundstrom, A. M., Guo, Y. S., Lipponen, A., Kokkonen, T. V.,

827 Kontkanen, J., Cai, R. L., Cai, J., Chan, T., Chen, L. D., Chu, B. W., Deng, C. J., Du, W., Fan, X. L., He, X. C., Kangasluoma, J., Kujansuu,

828 J., Kurppa, M., Li, C., Li, Y. R., Lin, Z. H., Liu, Y. L., Liu, Y. L., Lu, Y. Q., Nie, W., Pulliainen, J., Qiao, X. H., Wang, Y. H., Wen, Y.

829 F., Wu, Y., Yang, G., Yao, L., Yin, R. J., Zhang, G., Zhang, S. J., Zheng, F. X., Zhou, Y., Arola, A., Tamminen, J., Paasonen, P., Sun, Y.

830 L., Wang, L., Donahue, N. M., Liu, Y. C., Bianchi, F., Daellenbach, K. R., Worsnop, D. R., Kerminen, V. M., Petaja, T., Ding, A. J., Jiang,

831 J. K., and Kulmala, M.: The effect of COVID-19 restrictions on atmospheric new particle formation in Beijing, Atmos. Chem. Phys., 22,

832 12207-12220, https://doi.org/10.5194/acp-22-12207-2022, 2022.

833 Yan, X. Y., Akimoto, H., and Ohara, T.: Estimation of nitrous oxide, nitric oxide and ammonia emissions from croplands in East, Southeast

834 and South Asia, Glob. Change Biol., 9, 1080-1096, https://doi.org/10.1046/j.1365-2486.2003.00649.x, 2003.

835 Zhang, L., Shao, J., Lu, X., Zhao, Y., Hu, Y., Henze, D. K., Liao, H., Gong, S., and Zhang, Q.: Sources and Processes Affecting Fine

836 Particulate Matter Pollution over North China: An Adjoint Analysis of the Beijing APEC Period, Environ. Sci. Technol., 50, 8731-8740,

837 https://doi.org/10.1021/acs.est.6b03010, 2016.

838 Zhang, Q., Pan, Y., He, Y., Walters, W. W., Ni, Q., Liu, X., Xu, G., Shao, J., and Jiang, C.: Substantial nitrogen oxides emission reduction

839 from China due to COVID-19 and its impact on surface ozone and aerosol pollution, Sci. Total Environ., 753, 142238,

840 https://doi.org/10.1016/j.scitotenv.2020.142238, 2021.

841 Zhang, R. X., Zhang, Y. Z., Lin, H. P., Feng, X., Fu, T. M., and Wang, Y. H.: NOx Emission Reduction and Recovery during COVID-19 in

842 East China, Atmosphere, 11, 15, https://doi.org/10.3390/atmos11040433, 2020.

843 Zhang, W., Guo, J. H., Sun, Y. L., Yuan, H., Zhuang, G. S., Zhuang, Y. H., and Hao, Z. P.: Source apportionment for,urban PM10 and PM2.5

844 in the Beijing area, Chin. Sci. Bull., 52, 608-615, https://doi.org/10.1007/s11434-007-0076-5, 2007.

845 Zhao, X., Wang, G., Wang, S., Zhao, N., Zhang, M., and Yue, W.: Impacts of COVID-19 on air quality in mid-eastern China: An insight into

846 meteorology and emissions, Atmos. Environ., 266, 118750, https://doi.org/10.1016/j.atmosenv.2021.118750, 2021.

847 Zhao, Y. B., Zhang, K., Xu, X. T., Shen, H. Z., Zhu, X., Zhang, Y. X., Hu, Y. T., and Shen, G. F.: Substantial Changes in Nitrogen Dioxide

848 and Ozone after Excluding Meteorological Impacts during the COVID-19 Outbreak in Mainland China, Environ. Sci. Technol. Lett., 7,

849 402-408, https://doi.org/10.1021/acs.estlett.0c00304, 2020.

850 Zheng, B., Zhang, Q., Geng, G., Chen, C., Shi, Q., Cui, M., Lei, Y., and He, K.: Changes in China's anthropogenic emissions and air quality

851 during the COVID-19 pandemic in 2020, Earth Syst. Sci. Data, 13, 2895-2907, https://doi.org/10.5194/essd-13-2895-2021, 2021.

852 Zheng, B., Tong, D., Li, M., Liu, F., Hong, C. P., Geng, G. N., Li, H. Y., Li, X., Peng, L. Q., Qi, J., Yan, L., Zhang, Y. X., Zhao, H. Y.,

853 Zheng, Y. X., He, K. B., and Zhang, Q.: Trends in China's anthropogenic emissions since 2010 as the consequence of clean air actions,

854 Atmos. Chem. Phys., 18, 14095-14111, https://doi.org/10.5194/acp-18-14095-2018, 2018.

855 Zuo, P. J., Zong, Z., Zheng, B., Bi, J. Z., Zhang, Q. H., Li, W., Zhang, J. W., Yang, X. Z., Chen, Z. G., Yang, H., Lu, D. W., Zhang, Q. H.,

856 Liu, Q., and Jiang, G. B.: New Insights into Unexpected Severe PM2.5 Pollution during the SARS and COVID-19 Pandemic Periods in

857 Beijing, Environ. Sci. Technol., 56, 155-164, https://doi.org/10.1021/acs.est.1c05383, 2022.